## A FAMILY OF IMMERSED FINITE ELEMENT SPACES AND APPLICATIONS TO THREE-DIMENSIONAL H(curl) INTERFACE PROBLEMS\*

LONG CHEN<sup>†</sup>, RUCHI GUO<sup>‡</sup>, AND JUN ZOU<sup>§</sup>

Abstract. Efficient and accurate computation of  $\mathbf{H}(\text{curl})$  interface problems is of great importance in many electromagnetic applications. Unfitted mesh methods are especially attractive in three-dimensional (3D) computation as they can circumvent generating complex 3D interface-fitted meshes. However, many unfitted mesh methods rely on nonconforming approximation spaces, which may cause a loss of accuracy for solving Maxwell-type equations, and the widely used penalty techniques in the literature may not help in recovering the optimal convergence. In this article, we provide a remedy by developing Nédélec-type immersed finite element (IFE) spaces with a Petrov–Galerkin scheme that is able to produce optimal-convergent solutions. To establish a systematic framework, we analyze all the  $H^1$ ,  $\mathbf{H}(\text{curl})$ , and  $\mathbf{H}(\text{div})$  IFE spaces and form a discrete de Rham complex. Based on these fundamental results, we further develop a fast solver using a modified Hiptmair–Xu preconditioner which works for both the generalized minimal residual (GMRES) and conjugate gradient (CG) methods for solving the nonsymmetric linear algebraic system. The approximation capabilities of the proposed IFE spaces will be also established.

**Key words.** interface problems, Maxwell equations, immersed finite element methods, Petrov–Galerkin formulation, de Rham complex, Nédélec elements, Raviart–Thomas elements, preconditioner,  $\mathbf{H}(\operatorname{curl};\Omega)$ -elliptic equations

MSC codes. 65N12, 65N15, 65N30, 65N55

**DOI.** 10.1137/22M1505360



1. Introduction. Efficient and accurate computation of electromagnetic interface problems is of great importance since many applications involve multiple media with different electromagnetic properties, such as electromagnetic motors and actuators for electric drive vehicles [12, 35], and some nondestructive detection techniques based on electromagnetic fields [1, 24].

Let  $\mathbf{u}$  be an electric or magnetic field in a domain  $\Omega$  in  $\mathbb{R}^3$  that covers multiple subdomains representing media with different electromagnetic properties. For simplicity, we assume that there are only two subdomains of  $\Omega$  denoted as  $\Omega^{\pm}$  separated by an interface  $\Gamma$ . Then, the mathematical model for the interface conditions of  $\mathbf{u}$  at  $\Gamma$  can be generally written as

<sup>\*</sup>Submitted to the journal's Methods and Algorithms for Scientific Computing section June 27, 2022; accepted for publication (in revised form) April 11, 2023; published electronically December 15, 2023.

https://doi.org/10.1137/22M1505360

**Funding:** The work of the first author was funded by NSF DMS-2012465 and DMS-2309785. The second author was funded by NSF DMS-2309777. The work of the second author was supported in part by HKSAR grant 15302120. The work of the third author was substantially supported by Hong Kong RGC General Research Fund (projects 14306921 and 14306719).

<sup>&</sup>lt;sup>†</sup>Department of Mathematics, University of California at Irvine, Irvine, CA 92697 USA (chenlong@uci.edu).

<sup>&</sup>lt;sup>‡</sup>Department of Mathematics, University of California at Irvine, Irvine, CA 92697 USA, The Chinese University of Hong Kong, Hong Kong (ruchig@uci.edu).

 $<sup>^{\</sup>S}$  Department of Mathematics, The Chinese University of Hong Kong, Shatin, N.T., Hong Kong (zou@math.cuhk.edu.hk).

$$[\mathbf{u} \times \mathbf{n}]_{\Gamma} := \mathbf{u}^{+} \times \mathbf{n} - \mathbf{u}^{-} \times \mathbf{n} = \mathbf{0},$$

(1.1b) 
$$[(\alpha \operatorname{curl} \mathbf{u}) \times \mathbf{n}]_{\Gamma} := \alpha^{+} \operatorname{curl} \mathbf{u}^{+} \times \mathbf{n} - \alpha^{-} \operatorname{curl} \mathbf{u}^{-} \times \mathbf{n} = \mathbf{0},$$

(1.1c) 
$$[\beta \mathbf{u} \cdot \mathbf{n}]_{\Gamma} := \beta^{+} \mathbf{u}^{+} \cdot \mathbf{n} - \beta^{-} \mathbf{u}^{-} \cdot \mathbf{n} = 0,$$

where **n** denotes the normal vector to  $\Gamma$  from  $\Omega^-$  to  $\Omega^+$ , and  $\alpha = \alpha^{\pm}$  and  $\beta = \beta^{\pm}$  in  $\Omega^{\pm}$  are assumed to be positive piecewise constant functions with different electromagnetic meanings in various situations. In this work, we shall develop immersed finite element (IFE) spaces to capture those conditions.

The interface conditions in (1.1) appear in many formulations of Maxwell equations. For example, the following time-dependent curl-curl equation can be used to model an electric field  $\mathbf{u} = \mathbf{E}$ :

(1.2) 
$$\epsilon \mathbf{u}_{tt} + \sigma \mathbf{u}_t + \operatorname{curl}(\mu^{-1} \operatorname{curl} \mathbf{u}) = \mathbf{J}_t$$

subject to some boundary and initial conditions, where  $\epsilon$ ,  $\sigma$ , and  $\mu$  are the electric permeability, conductivity, and magnetic permeability of the media, respectively, and **J** is the applied current density. Then, solving (1.2) at each time step by an implicit method yields the **H**(curl) interface system

(1.3) 
$$\operatorname{curl}(\alpha \operatorname{curl} \mathbf{u}) + \beta \mathbf{u} = \mathbf{f}.$$

In this model, the jump conditions in (1.1) admit  $\alpha = \mu^{-1}$  and  $\beta = \epsilon \Delta t^{-2} + \sigma \Delta t^{-1}$ . We refer readers to [17, 27, 30, 47] for more details of this formulation.

It is widely known that traditional finite element (FE) methods can be applied on geometrically fitted meshes to solve interface problems, but generating a high-quality fitted mesh is nontrivial, especially for the considered three-dimensional (3D) space. For complex geometry, a global adjustment is needed to generate high-quality meshes, which can be computationally expensive. Locally modifying the mesh near the interface is more efficient [26, 28] but cannot guarantee shape regularity or even the maximal angle condition [14]. For arbitrarily shaped interface surfaces, the so-called slivers having edges nearly coplanar are difficult to completely remove from tetrahedral meshes [36], which may deteriorate the accuracy. For all these approaches, small edges of anisotropic meshes may make the conditioning of the resulting linear algebraic system even worse and pose a severer restriction on the time step size for time-dependent problems.

In contrast, some special numerical methods are designed for solving interface problems on unfitted meshes, which completely avoids the mesh generation issue. Typical examples include penalty-type methods [15, 16, 61], nonmatching mesh methods [21, 22, 27, 54], and IFE methods to be discussed in this article. The methodology of IFE methods is to encode the jump conditions in the construction of approximation spaces, i.e., the IFE spaces, which then have optimal approximation capabilities for functions satisfying the related jump conditions. We also refer readers to FDTD methods [77] based on a finite difference formulation for Maxwell interface equations. All these methods have been successfully applied to various interface problems arising from fluid, elasticity, wave propagation, and so on; see [6, 37, 39, 42, 45] and the references therein. However, due to the reason explained below, currently, there seems no satisfactory methodology for the Maxwell-type interface problems.

For almost all the aforementioned unfitted-mesh FE methods, one trade-off is the loss of the conformity of the approximation spaces. The proposed IFE space is also  $\mathbf{H}(\text{curl})$ -nonconforming, i.e., not tangential continuous across interface faces;

see Figure 3.1 for an illustration. For many situations, the discontinuity can be well handled by suitable penalties such as Nitsche's penalty [15, 60]. The essential idea is to treat those spaces through a discontinuous Galerkin (DG) formulation. But it becomes one of the main obstacles for Maxwell-type equations due to the underlying  $\mathbf{H}(\text{curl})$  space. Here let us briefly explain the issue. Solutions of (1.3) generally admit low regularity, especially near the interface [31, 32, 33]. Suppose that  $\mathbf{u} \in \mathbf{H}^s(\text{curl}; \Omega)$ , s > 0, and an approximation space is nonconforming on a face F; then the penalty  $h^{-1} \int_F [\mathbf{u}_h \times \mathbf{n}] \cdot [\mathbf{v}_h \times \mathbf{n}] \, ds$  is generally needed to ensure the stabilization. As a result, in the error estimation, one needs the inequality

(1.4) 
$$h_K^{-1/2} \|\mathbf{u} - \pi_F \mathbf{u}\|_{L^2(F)} \lesssim h_K^{s-1} \|\mathbf{u}\|_{\mathbf{H}^s(\operatorname{curl};K)},$$

where  $\pi_F$  is a projection to some polynomial space on F. The inequality in (1.4) will not cause any issue if the solution regularity is high enough; see the recent work [61]. In [61], the authors developed a framework of penalty-type methods for all the  $H^1$ ,  $\mathbf{H}(\text{curl})$ , and  $\mathbf{H}(\text{div})$  interface problems that can uniformly handle arbitrarily high order spaces. The penalty idea was also employed for unfitted mesh methods based on a patch-reconstruction technique in [59]. However, note that even for a moderate regularity s = 1, (1.4) immediately leads to a failure of convergence. This issue has been studied in a series of articles in the literature [9, 21, 22, 69], and it seems to be essential rather than caused by the limitation of analysis techniques as it can be verified numerically in the aforementioned works.

Some approaches in the literature can overcome this issue. One is to search for a conforming subspace of the underlying nonconforming space, including standard DG methods [51, 52] and the mortar FE method [54] relying on a "nested mesh" assumption. As the unfitted mesh methods modify their spaces near the interface, the conforming subspaces may not exist. Without resorting to conformity, some approaches can use the appropriate scaling in the stabilization [7, 13, 19] to overcome this issue. But for many unfitted mesh methods, such a scaling factor may not yield a stable scheme.

Therefore, it would be highly desirable if the penalty could be completely avoided. With this motivation, here we employ a Petrov–Galerkin (PG) formulation that uses IFE trial spaces but keeps the standard conforming FE test spaces, which addresses the nonconformity issue by avoiding estimate (1.4). For the resulting matrix being square, the trial and test spaces should have the same number of degrees of freedom (DoFs). Thus, we shall design the IFE spaces to be isomorphic to the standard FE spaces through the usual DoFs, which is shown by the mapping between the middle and bottom sequences in Figure 1.1; see the definition of the spaces and operators in section 3.3. The original idea of PG formulation can be found in the fundamental work [3] of Babuška, Caloz, and Osborn and is then used in [50] for the multiscale FE method and in [49] for IFE methods on  $H^1$  interface problems.

There are multiple novelties in this work. We construct both the 3D  $\mathbf{H}(\text{curl})$  and  $\mathbf{H}(\text{div})$  IFE spaces according to their corresponding jump conditions and show that they have the same edge and face DoFs as the standard Nédélec and Raviart-Thomas elements, respectively. Although the local IFE spaces have been introduced in [20], we establish a few fundamental properties including unisolvence, approximation capabilities, and the de Rham complex, as shown by the middle sequence in Figure 1.1 that is identical to the FE counterparts. The resulting PG-IFE method has the optimal convergence, and its condition number is independent of small-cutting elements.

There have been extensive works on developing efficient preconditioners for unfitted mesh methods for various interface problems; see [38, 34, 62, 73]. However, to

FIG. 1.1. Diagrams of IFE spaces.  $S_h^{\mathbf{r}}, \mathbf{S}_h^{e}$ , and  $\mathbf{S}_h^{f}$  are IFE spaces.  $\widetilde{S}_h^{\mathbf{r}}, \widetilde{\mathbf{S}}_h^{e}$ , and  $\widetilde{\mathbf{S}}_h^{f}$  are standard FE spaces. They are isomorphisms through the canonical interpolation operators defined by DoFs.

the best of our knowledge, there seems to be no study on preconditioners for those methods on the  $\mathbf{H}(\text{curl})$  system. In fact, it is well known that solving the linear algebraic system from the  $\mathbf{H}(\text{curl})$  system is challenging, as the kernel space of the curl operator is quite large. An exact sequence is demanded to describe the kernel space precisely. In this paper, based on the de Rham complex, we develop an IFE version of the HX preconditioner [48]. We design a special smoother by computing the exact inverse of the non-SPD submatrix near the interface. The idea is closely related to domain decomposition methods [76]. We demonstrate by numerical experiments that the resulting fast solver works well for generalized minimal residual (GMRES) methods and even conjugate gradient (CG) methods which typically do not converge for non-SPD systems. It is worthwhile to mention that CG-like methods have been developed for more general semisymmetric matrices [63]. We also refer readers to multigrid methods for  $H^1$ -interface problems in [75, 53].

The article contains six additional sections. In the next section, we describe the geometry and set up some notation. In section 3, we establish the IFE spaces and their de Rham complex. In section 4, we describe the PG-IFE formulation, the fast solver, and a numerical test for the *inf-sup* condition. In section 5, we show the optimal approximation capabilities. In section 6, we present some numerical experiments. In section 7, we offer some concluding remarks.

- 2. Preliminary. In this section, we describe an unfitted background mesh and introduce some spaces and notation which will be frequently used in this paper.
- **2.1.** Meshes. An electromagnetic wave generally propagates over the whole space, and a widely used approach is to cover the modeling media by a box as a modeling and computational domain. So in this paper, we shall assume our domain is cubic and generate a background Cartesian mesh in which each cubic element is then partitioned into several tetrahedra. For example, we show two types of triangulations in the left two plots of Figure 2.1, where the triangulation in Type I does not introduce extra nodes, but Type II introduces an extra node on each face and one inside the element. (We show only 4 tetrahedra in the second plot of Figure 2.1 for better illustration). All these tetrahedra form an interface-unfitted shape-regular mesh denoted by  $\mathcal{T}_h$  which will be used for discretization. Let  $\mathcal{N}_h$ ,  $\mathcal{E}_h$ , and  $\mathcal{F}_h$  be the collection of nodes, edges, and faces of  $\mathcal{T}_h$ , respectively. For each element K, we let  $\mathcal{N}_K$ ,  $\mathcal{E}_K$ , and  $\mathcal{F}_K$  be the collection of nodes, edges, and faces of K with  $|\mathcal{N}_K| = 4$ ,  $|\mathcal{E}_K| = 6$ , and  $|\mathcal{F}_K| = 4$ .

Given the signed-distance level-set function of the interface denoted by  $\varphi^{\Gamma}$ , we can compute its linear interpolation  $\varphi_h^{\Gamma}$  on the mesh  $\mathcal{T}_h$ ; namely,  $\varphi_h^{\Gamma}$  interpolates  $\varphi^{\Gamma}$  at



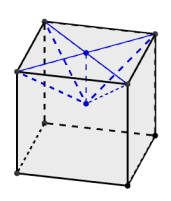
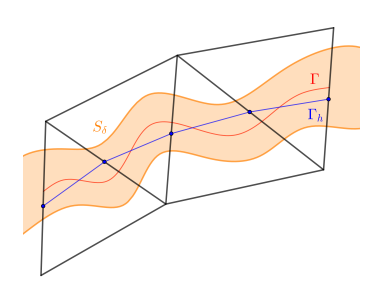






FIG. 2.1. Triangulation of a cube. The left two plots show two triangulation approaches resulting in 5 tetrahedra (Type I) and 24 tetrahedra (Type II). The right two plots show two types of tetrahedra from the triangulation: a trirectangular tetrahedron, which is a tetrahedron that has three isometric orthogonal edges meeting at one vertex, and a regular tetrahedron, whose edges have equal length.



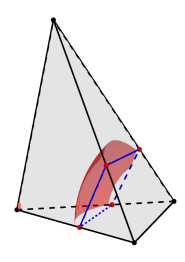


FIG. 2.2. An illustration of the mismatching region of an element and the  $\delta$  strip. The intersection points of  $\Gamma_h^K$  are always coplanar, while those of  $\Gamma$  may not be.

the mesh nodes and is piecewise linear on each element. Then, the numerical interface is defined as

(2.1) 
$$\Gamma_h = \{ \mathbf{x} : \varphi_h^{\Gamma}(\mathbf{x}) = 0 \}.$$

We note that as  $\varphi_h^{\Gamma}$  is piecewise linear,  $\Gamma_h$  is also piecewise linear and forms a polyhedron as a linear approximation to the exact interface. See Figure 2.2 for illustration. Linear interpolation of signed-distance functions has been widely used for discretizing interface numerically [71, 67]. Note that  $\Gamma_h$  may not be the linear interpolation of  $\Gamma$ . For a smooth interface, the geometric error is still in the order of  $\mathcal{O}(h^2)$  (see Lemma 5.3), which is sufficient for a linear method [58]. Then, we let  $\Gamma_h$  cut  $\Omega$  into  $\Omega_h^{\pm}$ . An element K is called an interface element if

(2.2) 
$$\min_{\mathbf{x} \in \mathcal{N}_K} \varphi_h^{\Gamma}(\mathbf{x}) \max_{\mathbf{x} \in \mathcal{N}_K} \varphi_h^{\Gamma}(\mathbf{x}) < 0.$$

As  $\varphi_h^{\Gamma}$  interpolates  $\varphi^{\Gamma}$  at the mesh nodes, (2.2) also implies that K intersects the exact interface. Let  $\mathcal{T}_h^i$  be the collection of interface elements. In addition, given a  $K \in \mathcal{T}_h^i$ , define the interface patch  $\Gamma_h^K = \Gamma_h \cap K$ . Let  $K_h^{\pm}$  be the two subelements cut by the interface patch  $\Gamma_h^K$ .

**2.2. Sobolev Spaces.** Given a subdomain  $D \subseteq \Omega$ , for a nonnegative number s, we let  $H^s(D)$  be the standard Sobolev space. In addition, we introduce the following vector function spaces:

(2.3a) 
$$\mathbf{H}^{s}(\operatorname{curl}; D) = \{ \mathbf{u} \in \mathbf{H}^{s}(D) : \operatorname{curl} \mathbf{u} \in \mathbf{H}^{s}(D) \},$$

(2.3b) 
$$\mathbf{H}^{s}(\operatorname{div}; D) = \{\mathbf{u} \in \mathbf{H}^{s}(D) : \operatorname{div} \mathbf{u} \in H^{s}(D)\}.$$

Given a subdomain  $D \subseteq \Omega$ , if  $D \cap \Gamma \neq \emptyset$ , we let  $D^{\pm} = \Omega^{\pm} \cap D$  and further denote  $H^s(\cup D^{\pm})$ ,  $\mathbf{H}^s(\operatorname{curl}; \cup D^{\pm})$ , and  $\mathbf{H}^s(\operatorname{div}; \cup D^{\pm})$  consisting of functions that belong to the corresponding Sobolev spaces on each  $D^{\pm}$ . Given a face F in the mesh, we let  $\operatorname{rot}_F$  be the two-dimensional (2D) rotatory operator on F and define the space

(2.4) 
$$\mathbf{H}^s(\operatorname{rot};F) = \{ \mathbf{u} \in \mathbf{H}^s(F) : \operatorname{rot}_F \mathbf{u} \in H^s(F) \}.$$

The  $H^1$ -interface problem reads as

(2.5) 
$$-\nabla \cdot (\beta \nabla u) = f \quad \text{in } \Omega^- \cup \Omega^+,$$

with  $f \in L^2(\Omega)$ , subject to u = 0 on  $\partial \Omega$  and the jump conditions

(2.6a) 
$$[u]_{\Gamma} := u^{+} - u^{-} = 0,$$

(2.6b) 
$$[\beta \nabla u \cdot \mathbf{n}]_{\Gamma} := \beta^{+} \nabla u^{+} \cdot \mathbf{n} - \beta^{-} \nabla u^{-} \cdot \mathbf{n} = 0,$$

where the parameter  $\beta$  is the same as the one in (1.1c) that has a similar physical meaning related to conductivity. The  $\mathbf{H}(\text{div})$ -interface problem is given by

$$-\nabla \operatorname{div}(\mathbf{u}) + \alpha \mathbf{u} = \mathbf{f},$$

with  $\mathbf{f} \in \mathbf{H}(\operatorname{curl}; \Omega)$ , subject to  $\mathbf{u} \cdot \mathbf{n} = 0$  on  $\partial \Omega$  and the jump conditions

$$[\mathbf{u} \cdot \mathbf{n}]_{\Gamma} := \mathbf{u}^+ \cdot \mathbf{n} - \mathbf{u}^- \cdot \mathbf{n} = 0,$$

(2.8b) 
$$[\alpha \mathbf{u} \times \mathbf{n}]_{\Gamma} := \alpha^{+} \mathbf{u}^{+} \times \mathbf{n} - \alpha^{-} \mathbf{u}^{-} \times \mathbf{n} = \mathbf{0},$$

$$[\operatorname{div}(\mathbf{u})]_{\Gamma} := \operatorname{div}(\mathbf{u}^{+}) - \operatorname{div}(\mathbf{u}^{-}) = 0.$$

This system comes from the first-order least-squares formulation of the elliptic interface problem [18] or preconditioning for the mixed FE using a gradient formulation [2]. The related FE approximation for interface problems can be found in [46].

Now we encode the jump conditions for the  $H^1$  case (2.6), the  $\mathbf{H}(\text{curl})$  case (1.1), and the  $\mathbf{H}(\text{div})$  case (2.8) into the definition of the following special Sobolev spaces:

(2.9a) 
$$H^{2}(\beta; D) := \{ u \in H^{2}(\cup D^{\pm}) \cap H^{1}(D) : \beta \nabla u \in \mathbf{H}(\operatorname{div}; D) \},$$

(2.9b) 
$$\mathbf{H}^{1}(\alpha, \beta, \operatorname{curl}; D) := \{ \mathbf{u} \in \mathbf{H}^{1}(\operatorname{curl}; \cup D^{\pm}) \cap \mathbf{H}(\operatorname{curl}; D) :$$

$$\beta \mathbf{u} \in \mathbf{H}(\operatorname{div}; D), \ \alpha \operatorname{curl} \mathbf{u} \in \mathbf{H}(\operatorname{curl}; D) \},$$

(2.9c) 
$$\mathbf{H}^{1}(\alpha, \operatorname{div}; D) := \{ \mathbf{u} \in \mathbf{H}^{1}(\operatorname{div}; \cup D^{\pm}) \cap \mathbf{H}(\operatorname{div}; D) : \alpha \mathbf{u} \in \mathbf{H}(\operatorname{curl}; D), \operatorname{div} \mathbf{u} \in H^{1}(D) \}.$$

An alternative interpretation of these interface conditions is to regard  $\alpha$  and  $\beta$  as Hodge star operators mapping between fields in different Sobolev spaces, which is illustrated by the following diagram (2.10). The construction of IFE spaces is just to mimic the diagram locally on each interface element.

3. Immersed finite element spaces. In this section, we develop Nédélec-type and Raviart-Thomas-type IFE spaces that admit the edge and face DoFs, respectively. We shall use  $\alpha_h$  and  $\beta_h$  for the discontinuous coefficients partitioned by  $\Gamma_h$  instead of  $\Gamma$ . In the following discussion, we let  $\mathbb{P}_k(D)$  be the kth degree polynomial space on a domain D. For the sake of the readers, we recall the lowest-order local Nédélec [65, 66] and Raviart-Thomas spaces [68]:

$$\mathcal{ND}_0(K) := \{ \mathbf{a} \times \mathbf{x} + \mathbf{b} : \mathbf{a} \in \mathbb{R}^3, \ \mathbf{b} \in \mathbb{R}^3 \},$$
$$\mathcal{RT}_0(K) := \{ c \mathbf{x} + \mathbf{a} : c \in \mathbb{R}, \ \mathbf{a} \in \mathbb{R}^3 \}.$$

The local 3D  $H^1$  IFE space has been constructed in [57], and the  $\mathbf{H}(\text{div})$  and  $\mathbf{H}(\text{curl})$  can be found in a recent work [20], which will be reviewed in section 3.1. However, this work does not show any DoFs of these local spaces and the related unisolvence. A typical continuous-type Galerkin scheme requires the usual nodal, edge, and face DoFs to glue those local spaces together. This is also crucial for the proposed PG formulation. In section 3.2, we analyze those DoFs with unisolvence and point out that this is highly nontrivial due to the jump conditions. In fact, unlike the usual FE spaces, the unisolvence demands certain geometrical conditions of the elements. Finally, we establish the de Rham complex for these spaces.

3.1. The local  $H^1$ , H(curl), and H(div) IFE spaces. Consider the two piecewise constant vector spaces

$$(3.1a) \quad \mathbf{A}_h(K) = \{ \mathbf{c} : \mathbf{c}^{\pm} = \mathbf{c}|_{K_h^{\pm}} \in \left[ \mathbb{P}_0(K_h^{\pm}) \right]^3, \ \mathbf{c} \in \mathbf{H}(\mathrm{div}; K), \ \alpha_h \mathbf{c} \in \mathbf{H}(\mathrm{curl}; K) \},$$

$$(3.1b) \quad \mathbf{B}_h(K) = \{ \mathbf{c} : \mathbf{c}^{\pm} = \mathbf{c}|_{K_h^{\pm}} \in \left[ \mathbb{P}_0(K_h^{\pm}) \right]^3, \ \mathbf{c} \in \mathbf{H}(\operatorname{curl}; K), \ \beta_h \mathbf{c} \in \mathbf{H}(\operatorname{div}; K) \}.$$

We can derive the specific format for functions in (3.1). Given each interface element with the approximate plane  $\Gamma_h^K$ , we let  $\bar{\mathbf{n}}_K$ ,  $\bar{\mathbf{t}}_{K,1}$ , and  $\bar{\mathbf{t}}_{K,2}$  be its unit normal vector and two orthogonal unit tangential vectors. Furthermore, we denote  $T_K = [\bar{\mathbf{n}}_K, \bar{\mathbf{t}}_{K,1}, \bar{\mathbf{t}}_{K,2}]$  and define the transformation matrices

$$(3.2) \hspace{1cm} A_K = T_K \left[ \begin{array}{ccc} 1 & 0 & 0 \\ 0 & \tilde{\alpha} & 0 \\ 0 & 0 & \tilde{\alpha} \end{array} \right] T_K^\top \hspace{0.1cm} \text{and} \hspace{0.1cm} B_K = T_K \left[ \begin{array}{ccc} \tilde{\beta} & 0 & 0 \\ 0 & 1 & 0 \\ 0 & 0 & 1 \end{array} \right] T_K^\top,$$

where  $\tilde{\alpha} = \alpha^+/\alpha^-$  and  $\tilde{\beta} = \beta^+/\beta^-$ . Then, the spaces  $\mathbf{A}_h(K)$  and  $\mathbf{B}_h(K)$  can be rewritten as

$$\mathbf{A}_h(K) = \{ \mathbf{c} : \mathbf{c}^{\pm} \in \left[ \mathbb{P}_0(K_h^{\pm}) \right]^3, \ \mathbf{c}^- = A_K \mathbf{c}^+ \},$$

$$\mathbf{B}_h(K) = \{ \mathbf{c} : \mathbf{c}^{\pm} \in \left[ \mathbb{P}_0(K_h^{\pm}) \right]^3, \ \mathbf{c}^- = B_K \mathbf{c}^+ \}.$$

With these two piecewise constant vector spaces, we are able to construct the  $H^1$ ,  $\mathbf{H}(\operatorname{curl})$ , and  $\mathbf{H}(\operatorname{div})$  IFE spaces, denoted by  $S_h^n(K)$ ,  $\mathbf{S}_h^e(K)$ , and  $\mathbf{S}_h^f(K)$ , which are reported in Table 3.1 including their corresponding jump conditions and general function format. One can easily check that the IFE spaces above belong to the corresponding Sobolev spaces. The jump conditions for functions in  $\mathbf{S}_h^e(K)$  or  $\mathbf{S}_h^f(K)$  are satisfied only at one point  $\mathbf{x}_K$ . Moreover, the formats are identical to the standard Lagrange, Nédélec, and Raviart–Thomas elements in which the only difference is the vectors  $\mathbf{a}_h$  and  $\mathbf{b}_h$  replacing the simple constant vectors in  $[\mathbb{P}_0(K)]^3$ . Then, it is easy to see the following exact sequence:

Table 3.1

The IFE spaces, the Sobolev spaces to which the IFE spaces belong, the IEF spaces' function format, and the jump conditions. Here,  $\mathbf{x}_K$  is chosen as the centroid of the interface patch  $\Gamma_h^K$ , but other choices are also acceptable; see Remark 3.1.

IFE spaces	$S_h^n(K)$	$\mathbf{S}_h^e(K)$	$\mathbf{S}_h^f(K)$
Sobolev spaces	$H^1(K)$	$\mathbf{H}(\operatorname{curl};K)$	$\mathbf{H}(\mathrm{div};K)$
Function	$\mathbf{b}_h \cdot (\mathbf{x} - \mathbf{x}_K) + c$	$\mathbf{a}_h \times (\mathbf{x} - \mathbf{x}_K) + \mathbf{b}_h$	$c(\mathbf{x} - \mathbf{x}_K) + \mathbf{a}_h$
format	$\mathbf{b}_h \in \mathbf{B}_h(K),$	$\mathbf{a}_h \in \mathbf{A}_h(K),$	$c \in \mathbb{P}_0(K)$ ,
	$c \in \mathbb{P}_0(K)$	$\mathbf{b}_h \in \mathbf{B}_h(K)$	$\mathbf{a}_h \in \mathbf{A}_h(K)$
Jump	$[v_h]_{\Gamma_h^K} = 0$	$\left[\mathbf{v}_{h} imesar{\mathbf{n}} ight]_{\Gamma_{1}^{K}}=0$	$[\mathbf{v}_h \cdot \bar{\mathbf{n}}]_{\Gamma_h^K} = 0$
conditions	$[\beta_h \nabla v_h \cdot \mathbf{\bar{n}}]_{\Gamma_h^K} = 0$	$[\beta_h \mathbf{v}_h \cdot \bar{\mathbf{n}}]_{\mathbf{x}_K}^n = 0$	$\left[\alpha_h \mathbf{v}_h \times \bar{\mathbf{n}}\right]_{\mathbf{x}_K}^n = 0$
	n	$[\alpha_h \operatorname{curl} \mathbf{v}_h \times \bar{\mathbf{n}}]_{\Gamma_h^K} = 0$	$[\operatorname{div} \mathbf{v}_h]_{\Gamma_h^K} = 0$

$$(3.3) \mathbb{R} \xrightarrow{\hookrightarrow} S_h^n(K) \xrightarrow{\operatorname{grad}} \mathbf{S}_h^e(K) \xrightarrow{\operatorname{curl}} \mathbf{S}_h^f(K) \xrightarrow{\operatorname{div}} \mathbb{P}_0(K) \to 0.$$

Remark 3.1. Our numerical experience and the analysis in section 5 show that  $\mathbf{x}_K$  can be quite arbitrary as long as it is located within the  $\mathcal{O}(h_K)$  distance to K. Indeed, different choices of  $\mathbf{x}_K$  generally lead to different IFE functions. In computation, we chose  $\mathbf{x}_K$  as the centroid of  $\Gamma_h^K$ . However, as an interesting observation, for the nodal IFE space, various  $\mathbf{x}_K$  in fact result in the same space, although the shape functions might be different. To see this, we take  $\mathbf{x}_K'$  as another point on  $\Gamma_h^K$ , and let  $\mathbf{t} = \mathbf{x}_K' - \mathbf{x}_K$ . Let us take the nodal space  $S_h^n(K)$  as an example. For any  $\mathbf{b}_h \in \mathbf{B}_h(K)$ , we have  $\mathbf{b}_h^- \cdot \bar{\mathbf{t}} = (\mathbf{b}_h^+)^\top B_K \bar{\mathbf{t}} = \mathbf{b}_h^+ \cdot \bar{\mathbf{t}}$ . Thus, a function  $v_h \in S_h^n(K)$  can be expressed as

(3.4) 
$$v_h = \mathbf{b}_h \cdot (\mathbf{x} - \mathbf{x}_K') + \mathbf{b}_h \cdot \bar{\mathbf{t}} + c = \mathbf{b}_h \cdot (\mathbf{x} - \mathbf{x}_K') + c',$$

showing that the functions defined with  $\mathbf{x}'_{K}$  also belong to  $S_{h}^{n}(K)$ .

**3.2. Degrees of freedom.** For the  $H^1$  case, it has been proved in [57] that the functions in  $S_h^n(K)$  admit nodal DoFs for the two types of tetrahedra shown in the right two plots of Figure 2.1, i.e., a trirectangular tetrahedron that has three isometric orthogonal edges meeting at one vertex and a regular tetrahedron that has six isometric edges. Namely, there exist  $\phi_i^n \in S_h^n(K)$ , i = 1, 2, 3, 4, such that  $\phi_i^n(\mathbf{z}_j) = \delta_{ij}$ , where  $\mathbf{z}_j$ , j = 1, 2, 3, 4, are the nodes of K. Then, the global  $H^1$  IFE space is defined as

$$S_h^n = \{ v_h \in L^2(\Omega) : v_h|_K \in S_h^n(K) \text{ if } K \in \mathcal{T}_h^i, \text{ and } v_h|_K \in \mathbb{P}_1(K) \text{ if } K \in \mathcal{T}_h^n,$$

$$(3.5) \qquad v_h \text{ is continuous at } \mathbf{x} \in \mathcal{N}_h \}.$$

We then consider the unisolvence of  $\mathbf{S}_h^f(K)$  and begin by deriving a formula for computing  $\mathbf{H}(\mathrm{div})$  IFE shape functions. Given an interface element K with 4 faces  $F_i$ ,  $i=1,2,\ldots,4$ , we introduce  $v_i=\int_{F_i}\mathbf{v}_h\cdot\mathbf{n}_{F_i}\,\mathrm{d}s$ , with  $\mathbf{n}_{F_i}$  being the unit normal vector to  $F_i$ , for any function  $\mathbf{v}_h=c(\mathbf{x}-\mathbf{x}_K)+\mathbf{a}_h\in\mathbf{S}_h^f(K)$  based on Table 3.1, and we let  $v_0=v_1+v_2+v_3+v_4$ . Determining c is straightforward:

(3.6) 
$$c = \frac{\operatorname{div}(\mathbf{v}_h)}{3} = \frac{1}{3|K|} \int_K \operatorname{div}(\mathbf{v}_h) \, d\mathbf{x} = \frac{1}{3|K|} \sum_{i=1}^4 \int_{F_i} \mathbf{v}_h \cdot \mathbf{n}_{F_i} \, ds = \frac{v_0}{3|K|}.$$

Then, by (3.1)  $\mathbf{a}_h$  should satisfy the following equations: for  $i = 1, \dots, 4$ ,

$$(3.7) |F_i^+|\mathbf{n}_{F_i}^\top \mathbf{a}_h^+ + |F_i^-|\mathbf{n}_{F_i}^\top A_K \mathbf{a}_h^+ = v_i - \frac{v_0}{3|K|} \int_{F_i} (\mathbf{x} - \mathbf{x}_K) \cdot \mathbf{n}_{F_i} \, \mathrm{d}s.$$

Imposing (3.7) on any three faces  $F_1$ ,  $F_2$ , and  $F_3$ , we obtain a linear system for  $\mathbf{a}_h^+$ :

(3.8) 
$$M_K \mathbf{a}_h^+ = \bar{\mathbf{v}}, \text{ with } M_K = \Phi^+ N_K + \Phi^- N_K A_K,$$

where  $\Phi^{\pm} = \operatorname{diag}(|F_1^{\pm}|, |F_2^{\pm}|, |F_3^{\pm}|), \ N_K = [\mathbf{n}_{F_1}, \mathbf{n}_{F_2}, \mathbf{n}_{F_3}]^{\top}$ , and  $\bar{\mathbf{v}}$  is given by the right-hand side of (3.7). The solvability of  $\mathbf{a}_h^+$  is equivalent to the invertibility of  $M_K$ .

LEMMA 3.2. Given a trirectangular tetrahedral or regular tetrahedral interface element K, the space  $\mathbf{S}_h^f(K)$  has the DoFs  $\int_{F_i} \mathbf{v}_h \cdot \mathbf{n}_{F_i} \, \mathrm{d}s$ , i = 1, 2, 3, 4.

*Proof.* It remains to show the invertibility of  $M_K$ . We treat the two types of tetrahedra separately.

If K is a trirectangular tetrahedron, we choose  $F_i$ , i = 1, 2, 3, as the three orthogonal faces. Then,  $N_K$  is an orthonormal matrix, and we can rewrite

$$(3.9) M_K N_K^{\top} = \Phi^+ + \Phi^- N_K A_K N_K^{\top} = \Phi \left( I + \Phi^{-1} \Phi^- N_K (A_K - I) N_K^{\top} \right),$$

where  $\Phi = \operatorname{diag}(|F_1|,|F_2|,|F_3|) = \Phi^- + \Phi^+$ . Without loss of generality, we can assume  $\tilde{\alpha} = \alpha^+/\alpha^- \le 1$ ; otherwise we simply consider the matrix  $M_K A_K^{-1} N_K^{\top} = \Phi^+ N_K A_K N_K^{\top} + \Phi^-$ . Let  $\lambda_{\max}(\cdot)$  be the largest magnitude of eigenvalues of a matrix. Note that  $\lambda_{\max}(\Phi^{-1}\Phi^-) \le 1$  and  $\lambda_{\max}(N_K (A_K - I) N_K^{\top}) = \lambda_{\max}(A_K - I) = 1 - \tilde{\alpha}$ . Since  $\Phi^{-1}\Phi^-$  is a diagonal matrix and  $N_K (A_K - I) N_K^{\top}$  is symmetric, it is well known that  $\Phi^{-1}\Phi^- N_K (A_K - I) N_K^{\top}$  has real eigenvalues, and

$$(3.10) \lambda_{\max}(\Phi^{-1}\Phi^{-}N_K(A_K - I)N_K^{\top}) \le \lambda_{\max}(\Phi^{-1}\Phi^{-})\lambda_{\max}(N_K(A_K - I)N_K^{\top}) \le 1 - \tilde{\alpha}.$$

Therefore, the eigenvalues of  $I + \Phi^{-1}\Phi^{-}N_K(A_K - I)N_K^{\top}$  must be bounded below by  $1 - (1 - \tilde{\alpha}) = \tilde{\alpha}$ , and thus, from (3.9), the matrix  $M_K$  is nonsingular.

If K is a regular tetrahedron, such a simple proof is not available. Instead, we employ a computer-aided argument to verify that  $M_K$  is nonsingular. As it is elementary and technical, we refer readers to the supplementary materials (120943\_1\_supp\_515743\_rq18d5\_sc.pdf [local/web 406KB]) for details.

Lemma 3.2 guarantees the existence of the shape functions  $\phi_i^f \in \mathbf{S}_h^f(K)$ , i = 1, 2, 3, 4, satisfying

(3.11) 
$$\int_{F_j} \phi_i^f \cdot \mathbf{n} \, ds = \delta_{ij}, \quad j = 1, 2, 3, 4,$$

regardless of interface location. Then, the global  $\mathbf{H}(\text{div})$  IFE space is defined as

$$\mathbf{S}_{h}^{f} = \left\{ \mathbf{v}_{h} \in L^{2}(\Omega) : \mathbf{v}_{h}|_{K} \in \mathbf{S}_{h}^{f}(K) \text{ if } K \in \mathcal{T}_{h}^{i}, \text{ and } \mathbf{v}_{h}|_{K} \in \mathcal{RT}_{0}(K) \text{ if } K \in \mathcal{T}_{h}^{n}, \right.$$

$$\left. \int_{F} [\mathbf{v}_{h} \cdot \mathbf{n}] \, \mathrm{d}s = 0 \, \forall F \in \mathcal{F}_{h} \right\}.$$

With the nodal and face DoFs, we are ready to analyze the DoFs of  $\mathbf{S}_h^e(K)$ .

LEMMA 3.3. Given a trirectangular tetrahedral or regular tetrahedral interface element K, the space  $\mathbf{S}_h^e(K)$  has the DoFs  $\int_{e_i} \mathbf{v}_h \cdot \mathbf{t}_i \, \mathrm{d}s$ ,  $i = 1, 2, \dots, 6$ .

*Proof.* Given an interface element K with six edges  $e_i$ , i = 1, ..., 6, we let  $v_i = \int_{e_i} \mathbf{v}_h \cdot \mathbf{t}_i \, \mathrm{d}s$  for a function  $\mathbf{v}_h \in \mathbf{S}_h^e(K)$  where  $\mathbf{t}_i$ 's have some assigned orientation. We need to show that  $\mathbf{v}_h$  uniquely exists for arbitrary  $v_i$ . As the dimensions match, we only need to prove the existence by explicitly constructing

(3.13) 
$$\boldsymbol{\phi}^e = \boldsymbol{\phi}^f \times (\mathbf{x} - \mathbf{x}_K)/2 + \nabla \phi^n,$$

satisfying the DoFs. For each face  $F_i$  of K, we let

(3.14) 
$$w_j = \sum_{e_i \subset \partial F_j} c_{j,e_i} v_i, \quad j = 1, \dots, 4, \text{ and } \phi^f = \sum_{j=1}^4 w_j \phi_j^f,$$

where  $c_{j,e_i} = 1$  or -1 is a sign to correct the orientation such that the edges associated with each face have the counterclockwise orientation. So, trivially  $\sum_{j=1}^{4} w_j = 0$  and thus  $\phi^f$  is div-free, i.e.,  $\phi^f \in \text{curl } \mathbf{S}_h^e(K)$  by the local exact sequence in (3.3). We then proceed to construct the component in  $S_h^n(K)$ . Let the four nodes of K be  $\mathbf{z}_l$ ,  $l = 1, \ldots, 4$ . Picking any node, say  $\mathbf{z}_4$ , without loss of generality, we let the three neighbor edges be  $e_i$  pointing to  $\mathbf{z}_i$ , i = 1, 2, 3. Define the orientation coefficients  $d_i = 1$  if  $\mathbf{t}_i$  points from  $\mathbf{z}_4$  to another ending point of  $\mathbf{e}_i$ ; otherwise  $d_i = -1$ . We then construct

$$\phi^n = \sum_{i=1,2,3} d_i \left( v_i - \int_{e_i} (\boldsymbol{\phi}^f \times (\mathbf{x} - \mathbf{x}_K)) \cdot \mathbf{t}_i / 2 \, \mathrm{d}s \right) \phi_i^n.$$

It is straightforward to see that  $\phi^e$  constructed in (3.13) matches the DoFs on  $e_i$ , i=1,2,3. The verification of the rest of the edges can be shown by the DoFs of  $\phi^f$  and  $\phi^n$  with the formula  $\int_F \operatorname{curl} \phi^e \cdot \mathbf{n} \, \mathrm{d}s = \int_F \operatorname{rot}_F \phi^e \, \mathrm{d}s = \int_{\partial F} \phi^e \cdot \mathbf{t} \, \mathrm{d}s$  for each face F.

Thanks to the same DoFs, the whole construction procedure exactly mimics the standard FE spaces. Lemma 3.3 guarantees the existence of Nédélec IFE shape functions  $\phi_i^e \in \mathbf{S}_b^e(K)$ , i = 1, 2, ..., 6, satisfying

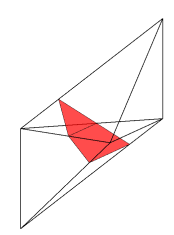
(3.15) 
$$\int_{e_i} \boldsymbol{\phi}_i^e \cdot \mathbf{t} \, \mathrm{d}s = \delta_{ij}, \quad j = 1, 2, \dots, 6.$$

Then, the global  $\mathbf{H}(\text{curl})$  IFE space can be constructed as

$$\mathbf{S}_{h}^{e} = \left\{ \mathbf{v}_{h} \in L^{2}(\Omega) : \mathbf{v}_{h}|_{K} \in \mathbf{S}_{h}^{e}(K) \text{ if } K \in \mathcal{T}_{h}^{i}, \text{ and } \mathbf{v}_{h}|_{K} \in \mathcal{ND}_{0}(K) \text{ if } K \in \mathcal{T}_{h}^{n}, \right.$$

$$\left. \int_{e} (\mathbf{v}_{h}|_{K_{1}} - \mathbf{v}_{h}|_{K_{2}}) \cdot \mathbf{t} \, \mathrm{d}s = 0 \, \forall e \in \mathcal{E}_{h}, \, \forall K_{1}, K_{2} \, \mathrm{sharing} \, e \right\}.$$

Remark 3.4. As  $\mathbf{v}_h \cdot \mathbf{t}$  is piecewise constant on  $e_h^{\pm}$ ,  $\int_e (\mathbf{v}_h|_{K_1} - \mathbf{v}_h|_{K_2}) \cdot \mathbf{t} \, \mathrm{d}s = 0$  cannot imply  $(\mathbf{v}_h|_{K_1} - \mathbf{v}_h|_{K_2}) \cdot \mathbf{t} = 0$ . So the IFE spaces are nonconforming. In fact, even the weak continuity  $\int_F (\mathbf{v}_h|_{K_1} - \mathbf{v}_h|_{K_2}) \times \mathbf{n}_F \, \mathrm{d}s = \mathbf{0}$  does not hold. We illustrate this kind of discontinuity in Figure 3.1 for an edge IFE function  $\mathbf{v}_h$  whose tangential traces  $\mathbf{v}_h|_{K_i} \times \mathbf{n}$  on F from the two neighboring elements,  $K_i$ , i = 1, 2, do not match.



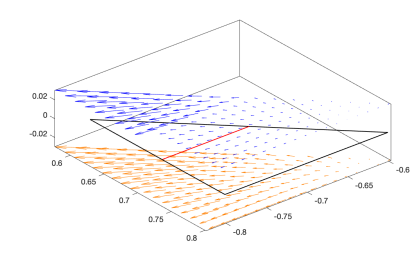


Fig. 3.1. Left: two neighbor elements. Right: the tangential traces of an IFE function on the sharing face from the two neighbor elements where the blue field is from the top and the orange field is from the bottom. (Color figure available online.)

Finally, we define the following interpolation operators:

$$\begin{split} I_h^n: H^2(\beta;\Omega) &\to S_h^n, & \text{satisfying } I_h^n u(\mathbf{x}) = u(\mathbf{x}) \ \forall \mathbf{x} \in \mathcal{N}_h, \\ I_h^e: \mathbf{H}^1(\alpha,\beta,\mathrm{curl};\Omega) &\to \mathbf{S}_h^e, & \text{satisfying } \int_e I_h^e \mathbf{u} \cdot \mathbf{t} \ \mathrm{d}s = \int_e \mathbf{u} \cdot \mathbf{t} \ \mathrm{d}s \ \forall e \in \mathcal{E}_h, \\ I_h^f: \mathbf{H}^1(\alpha,\mathrm{div};\Omega) &\to \mathbf{S}_h^f, & \text{satisfying } \int_F I_h^f \mathbf{u} \cdot \mathbf{n} \ \mathrm{d}s = \int_F \mathbf{u} \cdot \mathbf{n} \ \mathrm{d}s \ \forall F \in \mathcal{F}_h. \end{split}$$

Note that  $\int_{\mathcal{L}} \mathbf{u} \cdot \mathbf{t} \, ds$  is well defined since  $\mathbf{u}$  has piecewise  $\mathbf{H}^1(\text{curl})$  regularity.

**3.3.** The de Rham complex. Now we recover the well-known and important de Rham complex in Figure 1.1, where  $Q_h$  denotes the piecewise constant space on the mesh  $\mathcal{T}_h$ , and  $\Pi^0$  denotes the  $L^2$  projection to  $Q_h$ .

THEOREM 3.5. The sequence in the middle of Figure 1.1 is a complex.

*Proof.* First, it is clear that  $\mathbb{R} \subset S_h^n$ . In addition, with the local result in (3.3), we know that the functions mapped by the operators  $\nabla$ , curl, and div must satisfy the corresponding jump conditions on each element. Thus, we only need to verify the corresponding integral conditions on edges and faces in (3.16) and (3.12), respectively. For each edge  $e \in \mathcal{E}_h$  with the nodes  $\mathbf{z}_1$  and  $\mathbf{z}_2$ , we let  $K_1$  and  $K_2$  be any two elements sharing e. Then, given any  $v_h \in S_h^n$ , the continuity implies

$$\int_{e} \nabla v_{h}|_{K_{1}} \cdot \mathbf{t} \, \mathrm{d}s = v_{h}|_{K_{1}}(\mathbf{z}_{2}) - v_{h}|_{K_{1}}(\mathbf{z}_{1}) = v_{h}|_{K_{2}}(\mathbf{z}_{2}) - v_{h}|_{K_{2}}(\mathbf{z}_{1}) = \int_{e} \nabla v_{h}|_{K_{2}} \cdot \mathbf{t} \, \mathrm{d}s,$$

where **t** orients from  $\mathbf{z}_1$  to  $\mathbf{z}_2$ . So, we conclude  $\nabla v_h \in \mathbf{S}_h^e$ . Next, for each face  $F \in \mathcal{F}_h$ , we let  $K_1$  and  $K_2$  be the two neighbor elements. Given any  $\mathbf{v}_h \in \mathbf{S}_h^e$ , we have

$$\int_F \operatorname{curl} \mathbf{v}_h|_{K_1} \cdot \mathbf{n}_F \, \mathrm{d}s = \int_F \operatorname{rot}_F \mathbf{v}_h|_{K_1} \, \mathrm{d}s = \int_F \operatorname{rot}_F \mathbf{v}_h|_{K_2} \, \mathrm{d}s = \int_F \operatorname{curl} \mathbf{v}_h|_{K_2} \cdot \mathbf{n}_F \, \mathrm{d}s.$$

Therefore, we have  $\operatorname{curl} \mathbf{v}_h \in \mathbf{S}_h^f$ . Finally, it is trivial that  $\operatorname{div}(\mathbf{v}_h) \in Q_h$  for any  $\mathbf{v}_h \in \mathbf{S}_h^f$ .

Theorem 3.6. The diagram formed by the sequences in the middle and top of Figure 1.1 is commutative.

*Proof.* Let us only consider  $I_h^f \circ \text{curl} = \text{curl} \circ I_h^e$ , and the proof for other cases is similar. Given  $\mathbf{u} \in \mathbf{H}^1(\alpha, \beta, \text{curl}; \Omega)$ , there holds

$$\int_{F} I_{h}^{f} \operatorname{curl} \mathbf{u} \cdot \mathbf{n} \, \mathrm{d}s = \int_{F} \operatorname{curl} \mathbf{u} \cdot \mathbf{n} \, \mathrm{d}s = \int_{\partial F} \mathbf{u} \cdot \mathbf{t} \, \mathrm{d}s = \int_{\partial F} I_{h}^{e} \mathbf{u} \cdot \mathbf{t} \, \mathrm{d}s = \int_{F} \operatorname{curl} I_{h}^{e} \mathbf{u} \cdot \mathbf{n} \, \mathrm{d}s$$
 which finishes the proof.

To show the exactness, let us first describe the isomorphism between the IFE spaces and standard FE spaces. Let  $\widetilde{S}_h^n$ ,  $\widetilde{\mathbf{S}}_h^e$ , and  $\widetilde{\mathbf{S}}_h^f$  be the standard Lagrange, Nédélec, and Raviart—Thomas spaces defined on the same mesh  $\mathcal{T}_h$ . Note that the interpolations  $I_h^n$ ,  $I_h^e$ , and  $I_h^f$  are all well defined on these standard spaces, which lead to isomorphism; namely their inversions from the IFE spaces to FE spaces are also well defined. We shall keep the same notation  $I_h^n$ ,  $I_h^e$ , and  $I_h^f$  as the isomorphisms and illustrate this structure by the diagram formed from the middle and bottom sequences in 1.1, where I is the identity operator.

LEMMA 3.7. The diagram formed by the middle and bottom sequences in Figure 1.1 is commutative.

*Proof.* The argument is the same as for Theorem 3.6 by verifying the DoFs.

LEMMA 3.8. The operators  $I_h^n$ ,  $I_h^e$ , and  $I_h^f$  and their inversions preserve the kernels of  $\nabla$ , curl, and div:

$$(3.17) \qquad \ker(\mathbf{d}) \cap \widetilde{\mathbf{S}}_{h}^{s} \underset{(I_{h}^{s})^{-1}}{\overset{I_{h}^{s}}{\rightleftharpoons}} \ker(\mathbf{d}) \cap \mathbf{S}_{h}^{s}, \ (\mathbf{d}, s) = (\nabla, n), \ (\operatorname{curl}, e), \ (\operatorname{div}, f).$$

*Proof.* By the same argument of Theorem 3.6, we can show that the sequences in the middle and top of Figure 1.1 are commutative for both  $I_h^s$  and  $(I_h^s)^{-1}$ , which then implies the desired result.

Theorem 3.9. The sequence in the middle of Figure 1.1 is exact.

*Proof.* The result directly follows from Lemma 3.8 and the exactness for the standard FE spaces.  $\Box$ 

- 4. The Petrov–Galerkin IFE method for the  $\mathbf{H}(\text{curl})$  interface problem. In this section, we shall present the PG-IFE scheme by using the  $\mathbf{H}(\text{curl})$  IFE space as the trial space and the standard Nédélec FE space as the test space to the  $\mathbf{H}(\text{curl})$  interface problem. We then adapt the HX preconditioner for solving the resulting nonsymmetric linear algebraic system.
- **4.1. Schemes.** For simplicity of presentation, here we consider only the perfect electric conductor (PEC) or correspondingly the perfect magnetic conductor (PMC) boundary condition, i.e.,  $\mathbf{u} \times \mathbf{n} = \mathbf{0}$  on  $\partial \Omega$ . For the quasi-static equation (1.3), the proposed PG-IFE scheme is to find  $\mathbf{u}_h \in \mathbf{S}_{h,0}^e$ , i.e., the subspace of  $\mathbf{S}_h^e$  with the zero trace, such that

(4.1) 
$$a_h(\mathbf{u}_h, \mathbf{v}_h) = (\mathbf{f}, \mathbf{v})_{\Omega} \ \forall \mathbf{v}_h \in \widetilde{\mathbf{S}}_{h,0}^e$$
 with  $a_h(\mathbf{u}_h, \mathbf{v}_h) := (\alpha_h \operatorname{curl} \mathbf{u}_h, \operatorname{curl} \mathbf{v}_h)_{\Omega} + (\beta_h \mathbf{u}_h, \mathbf{v}_h)_{\Omega},$ 

where  $(\cdot, \cdot)_{\Omega}$  denotes the standard  $L^2$  inner product. Note that (4.1) follows from the integration by parts of (1.3) which always holds as long as the test function space is  $\mathbf{H}(\text{curl})$ -conforming. Thanks to the isomorphism between the IFE and FE spaces, the resulting linear system is square. So the PG formulation completely avoids the nonconformity issue mentioned in the introduction.

The PG scheme plays an important role in achieving optimal convergence. Let us briefly explain why the schemes with the H(curl)-nonconforming IFE space as the test function space with or without penalties all result in merely suboptimal convergence. Suppose  $\mathbf{u} \in \mathbf{H}^s(\alpha, \beta, \text{curl}; \Omega)$  is the exact solution. Testing (1.3) by  $\mathbf{v}_h \in \mathbf{S}_h^e$  and applying integration by parts yields

$$(4.2) \quad (\alpha \operatorname{curl} \mathbf{u}, \operatorname{curl} \mathbf{v}_h)_{\Omega} + (\beta \mathbf{u}, \mathbf{v}_h)_{\Omega} + \sum_{F \in \mathcal{F}_h^i} \int_F (\alpha \operatorname{curl} \mathbf{u}) \cdot [\mathbf{v}_h \times \mathbf{n}]_F \, \mathrm{d}s = (\mathbf{f}, \mathbf{v}_h)_{\Omega},$$

where  $\mathcal{F}_h^i$  denotes the collection of the faces intersecting with the interface, and  $[\cdot]_F$  denotes the jump of a quantity on F. The term of integration on faces in (4.2) appears as  $\mathbf{v}_h$  is generally not tangential continuous on F, which typically causes the loss of convergence. This is a widely observed issue for not just IFE methods [40, 43, 60] but also other unfitted mesh methods [15, 16, 21, 22], as almost all of them are built on nonconforming approximation spaces. A typical solution is to apply suitable penalties to handle the nonconformity. However, as the  $\mathbf{u}$  merely has the  $\mathbf{H}^s(\text{curl})$  regularity, the penalty terms, particularly the stabilization term will cause the suboptimal convergence shown in (1.4). We refer readers to [20] for a numerical example.

**4.2.** A fast solver: HX preconditioner. The resulting linear system of (4.1) is denoted by

$$\mathbf{B}^{PG}\bar{\mathbf{u}} = \bar{\mathbf{f}},$$

where  $\mathbf{B}^{PG}$  is not symmetric positive definite (SPD). However, the majority portion of  $\mathbf{B}^{PG}$  is indeed SPD, and the "problematic" portion is only around the interface. So, naturally, it may help if we employ the exact solver on the subsystem around the interface and use an iterative solver on the rest of the system. We shall apply the solver developed in our recent work [20] and briefly recall it below.

Define the collections of elements and edges around the interface:

(4.4) 
$$\mathcal{T}_{h}^{l} = \{ K \in \mathcal{T}_{h} : \overline{K} \cap \overline{K'} \neq \emptyset \text{ for some } K' \in \mathcal{T}_{h}^{l-1} \},$$
$$\mathcal{E}_{h}^{l} = \{ e \in \mathcal{E}_{h} : e \in \mathcal{E}_{K} \text{ for some } K \in \mathcal{T}_{h}^{l} \},$$

where  $\mathcal{T}_h^0 = \mathcal{T}_h^i$  is simply the set of interface elements. It is not hard to see that  $\mathcal{T}_h^l$  and  $\mathcal{E}_h^l$  can expand to the whole domain from the interface when increasing l. But with relatively small l, the set  $\mathcal{E}_h^l$  is sufficient to cover the "problematic" DoFs. Assuming that the DoFs associated with  $\mathcal{E}_h^l$  are indexed at the end, we can write

(4.5) 
$$\mathbf{B}^{PG} = \begin{bmatrix} \mathbf{B}_{l}^{(1,1)} & \mathbf{B}_{l}^{(2,1)} \\ \mathbf{B}_{l}^{(1,2)} & \mathbf{B}_{l}^{(2,2)} \end{bmatrix},$$

where  $\mathbf{B}_l^{(1,1)}$  is SPD but  $\mathbf{B}_l^{(2,2)}$  is non-SPD and also  $\mathbf{B}_l^{(1,2)} \neq (\mathbf{B}_l^{(2,1)})^{\top}$ . Based on (4.5), we then construct a special smoother:

(4.6) 
$$\mathbf{R}_{l}^{PG} = \begin{bmatrix} \operatorname{diag}(\mathbf{B}_{l}^{(1,1)}) & 0\\ 0 & \mathbf{B}_{l}^{(2,2)} \end{bmatrix},$$

In the following discussion,  $\mathbf{R}_l^{PG}$  and l shall be frequently referred to as a "block diagonal smoother" and an "expanding width," respectively.

We write  $\mathbf{B}^{\nabla}$  as the matrix associated with the IFE discretization of

$$(4.7) a_{h,1}^{\nabla}(\mathbf{u}_h, \mathbf{v}_h) := (\alpha_h \nabla \mathbf{u}_h, \nabla \mathbf{v}_h)_{\Omega} + (\beta_h \mathbf{u}_h, \mathbf{v}_h)_{\Omega} \quad \forall \mathbf{u}_h, \mathbf{v}_h \in [S_{h,0}^n]^3,$$

and write  $B^{\nabla}$  as the matrix of the bilinear form

$$(4.8) a_{h,2}^{\nabla}(u_h, v_h) := (\alpha_h \nabla u_h, \nabla v_h)_{\Omega} \quad \forall u_h, v_h \in S_{h,0}^n.$$

Then, the IFE version of the HX preconditioner [48] is

(4.9) 
$$\mathbf{B}^{\text{curl}} = [\mathbf{R}_l^{PG}]^{-1} + P_{\text{curl}}(\mathbf{B}^{\nabla})^{-1}P_{\text{curl}}^{\top} + G(B^{\nabla})^{-1}G^{\top}.$$

Here G is the matrix representation of the operator  $\nabla: \widetilde{S}_h^n \to \widetilde{\mathbf{S}}_h^e$ , which is indeed the incidence matrix between edges and vertices: there are two nonzero entries,  $\pm 1$ , on each row, and  $P_{\text{curl}}$  is the matrix associated with the interpolation operator  $\Pi_h^{\text{curl}}$ :  $[\widetilde{S}_h^n]^3 \to \widetilde{\mathbf{S}}_h^e$  such that  $\Pi_h^{\text{curl}} \mathbf{w}|_e \cdot \mathbf{t} = 0.5(\mathbf{w}_1 + \mathbf{w}_2) \cdot \mathbf{t} \ \forall e \in \mathcal{E}_h$  with  $\mathbf{w}_1$  and  $\mathbf{w}_2$  being the nodal values of  $\mathbf{w}$  at the nodes of e. We remark that these two matrices can be identically defined on the IFE spaces as the IFE spaces share exactly the same DoFs as the FE spaces. Hence, forming such matrices highly relies on the isomorphism shown in Figure 1.1. The matrices  $\mathbf{B}^{\nabla}$  and  $B^{\nabla}$  are SPD, and their inverses are approximated by a few algebraic multigrid (AMG) cycles. The  $[\mathbf{R}_l^{PG}]^{-1}$ , particularly the block  $(\mathbf{B}_l^{(2,2)})^{-1}$ , is computed by the direct solver (the backslash in MATLAB) as it is of small size, and we shall see that this direct solver only has a very subtle effect on the total computational time but is the key to handling the "problematic" DoFs near the interface. We adopt the HX preconditioner implemented in iFEM [25].

## **4.3.** A numerical test of the *inf-sup* condition. Define the energy norm

$$\|\mathbf{w}_h\|_{h,D}^2 = \int_D \alpha_h \operatorname{curl} \mathbf{w}_h \cdot \operatorname{curl} \mathbf{w}_h \, \mathrm{d}\mathbf{x} + \int_D \beta_h \mathbf{w}_h \cdot \mathbf{w}_h \, \mathrm{d}\mathbf{x} \quad \forall \mathbf{w}_h \in \mathbf{S}_h^e \text{ or } \widetilde{\mathbf{S}}_h^e.$$

Clearly, there holds the identity  $\|\mathbf{v}_h\|_{h,\Omega}^2 = a_h(\mathbf{v}_h, \mathbf{v}_h)$  and the norm equivalence  $\|\cdot\|_{\mathbf{H}(\operatorname{curl};\Omega)} \simeq \|\cdot\|_{h,\Omega}$ . With the optimal approximation capabilities of the  $\mathbf{H}(\operatorname{curl})$  IFE spaces discussed later, one can immediately show the optimal convergence for the PG-IFE scheme as long as the following *inf-sup* condition holds:

(4.10) 
$$\eta_s := \sup_{\mathbf{v}_h \in \widetilde{\mathbf{S}}_{h,0}^e} \frac{a_h(\mathbf{u}_h, \mathbf{v}_h)}{\|\mathbf{v}_h\|_{h,\Omega} \|\mathbf{u}_h\|_{h,\Omega}} \ge C_s \quad \forall \mathbf{u}_h \in \mathbf{S}_{h,0}^e.$$

However, it is generally quite challenging to show the *inf-sup* condition. The approach of Babuška, Caloz, and Osborn in [3] assumes a certain structure of the elliptic coefficient. The proof of the 2D PG-IFE method [41] highly relies on the symmetry of the high-order curl-curl term, which does not hold anymore for the 3D case. In this work, instead of pursuing a rigorous theoretical analysis, we provide a numerical test for the *inf-sup* condition (4.10).

Denote  $\mathbf{B}^{FE}$  and  $\mathbf{B}^{IF}$  as the matrices corresponding to the FE and IFE schemes on the same mesh, i.e., the matrices associated with the bilinear forms  $a_h(\mathbf{w}_h, \mathbf{v}_h)$ ,  $\mathbf{w}_h, \mathbf{v}_h \in \widetilde{\mathbf{S}}_{h,0}^e$  and  $a_h(\mathbf{w}_h, \mathbf{v}_h)$ ,  $\mathbf{w}_h, \mathbf{v}_h \in \mathbf{S}_{h,0}^e$ , respectively. Furthermore, we let N be the total number of edge DoFs. Then, (4.10) is equivalent to

(4.11) 
$$\sup_{\bar{\mathbf{v}} \in \mathbb{R}^N} \frac{\bar{\mathbf{v}}^{\top} \mathbf{B}^{PG} \bar{\mathbf{u}}}{\sqrt{\bar{\mathbf{u}}^{\top} \mathbf{B}^{IF} \bar{\mathbf{u}}} \sqrt{\bar{\mathbf{v}}^{\top} \mathbf{B}^{FE} \bar{\mathbf{v}}}} \ge C_s \quad \forall \bar{\mathbf{u}} \in \mathbb{R}^N.$$

In general, one may verify (4.11) by constructing a suitable test function  $\bar{\mathbf{v}} = \mathbf{P}\bar{\mathbf{u}}$ , where  $\mathbf{P}$  is a nonsingular matrix, such that

(4.12) 
$$\frac{\bar{\mathbf{u}}^{\top} \mathbf{P}^{\top} \mathbf{B}^{PG} \bar{\mathbf{u}}}{\sqrt{\bar{\mathbf{u}}^{\top} \mathbf{B}^{IF} \bar{\mathbf{u}}} \sqrt{\bar{\mathbf{u}}^{\top} \mathbf{P}^{\top} \mathbf{B}^{FE} \mathbf{P} \bar{\mathbf{u}}}} \ge C_s \quad \forall \bar{\mathbf{u}} \in \mathbb{R}^N.$$

It is not hard to see that (4.12) implies (4.14) as it takes sup over  $\bar{\mathbf{v}} \in \mathbb{R}^N$ . We shall focus on (4.12).

Note that one natural choice of the test function  $\mathbf{v}_h = (I_h^e)^{-1}\mathbf{u}_h$ . Consequently, in (4.12)  $\bar{\mathbf{u}} = \bar{\mathbf{v}}$ , i.e.,  $\mathbf{P}$  is an identity matrix, and thus an equivalent condition for (4.12) to hold is  $\mathbf{B}^{PG} + (\mathbf{B}^{PG})^{\top}$  being SPD. Unfortunately, numerical results show that  $\mathbf{B}^{PG} + (\mathbf{B}^{PG})^{\top}$  has negative eigenvalues. Our experience suggests that such a local construction approach may not be appropriate. Hence, we consider a global construction approach. Given each IFE function  $\mathbf{u}_h \in \mathbf{S}_{h,0}^e$ , we define its projection to the FE space denoted by  $\pi_h \mathbf{u}_h \in \widetilde{\mathbf{S}}_{h,0}^e$  through  $a_h(\cdot,\cdot)$ , namely

(4.13) 
$$a_h(\mathbf{u}_h, \mathbf{v}_h) = a_h(\pi_h \mathbf{u}_h, \mathbf{v}_h) \quad \forall \mathbf{v}_h \in \widetilde{\mathbf{S}}_{h,0}^e$$

Note that (4.13) is always well defined since  $a_h$  is SPD on the FE space. The corresponding vector solution of  $\pi_h \mathbf{u}_h$  is  $\bar{\mathbf{v}} = (\mathbf{B}^{FE})^{-1} \mathbf{B}^{PG} \bar{\mathbf{u}}$ , i.e.,  $\mathbf{P} = (\mathbf{B}^{FE})^{-1} \mathbf{B}^{PG}$ . Notice that

$$(4.14) \bar{\mathbf{u}}^{\mathsf{T}} \mathbf{P}^{\mathsf{T}} \mathbf{B}^{PG} \bar{\mathbf{u}} = \bar{\mathbf{u}}^{\mathsf{T}} (\mathbf{B}^{PG})^{\mathsf{T}} (\mathbf{B}^{FE})^{-1} \mathbf{B}^{PG} \bar{\mathbf{u}} = \bar{\mathbf{u}}^{\mathsf{T}} \mathbf{P}^{\mathsf{T}} \mathbf{B}^{FE} \mathbf{P} \bar{\mathbf{u}}.$$

Thus, (4.12) becomes the following minimization problem:

(4.15) 
$$\eta_s = \min_{\bar{\mathbf{u}} \in \mathbb{R}^N} \frac{\sqrt{\bar{\mathbf{u}}^\top (\mathbf{B}^{PG})^\top (\mathbf{B}^{FE})^{-1} \mathbf{B}^{PG} \bar{\mathbf{u}}}}{\sqrt{\bar{\mathbf{u}}^\top \mathbf{B}^{IF} \bar{\mathbf{u}}}}.$$

Similar to [5, 23], the solution to the minimization problem in (4.15) is the smallest generalized eigenvalue:

$$(4.16) (\mathbf{B}^{PG})^{\top} (\mathbf{B}^{FE})^{-1} \mathbf{B}^{PG} \bar{\mathbf{w}} = \lambda \mathbf{B}^{IF} \bar{\mathbf{w}}.$$

Here,  $\lambda$  must be nonnegative as the matrix on the left is semi-SPD and the right one is SPD. Thus, we have  $\eta_s = \sqrt{\lambda_{\min}}$  which can be used as a numerical estimate of the *inf-sup* constant. We refer readers to section 6 for the numerical results.

- 5. Approximation capabilities. In this section, we proceed to show the optimal approximation capabilities of the IFE spaces. Due to the interface conditions, it will be very different from the standard FE spaces in [30, 64]. Note that each subelement of an interface element can be highly irregular, and the desired error bounds should be independent of the irregular subelements, i.e., the generic constants are uniformly bounded regardless of how the interface cuts an element. This is one key difficulty in our analysis. In the following discussion, we shall employ the notation  $x \leq y$  to represent the relation  $x \leq Cy$ , where C is a generic constant that is independent of the irregular subelements. As the nodal interpolation of the  $H^1$  IFE space has been analyzed in [57], we shall concentrate on the  $\mathbf{H}(\text{curl})$  and  $\mathbf{H}(\text{div})$  cases here.
- **5.1. Some fundamental estimates.** Note that there is a mismatching region sandwiched by  $\Gamma_h$  and  $\Gamma$ . We denote it as  $K_{\text{int}} := (K^+ \cap K_h^-) \cup (K^- \cap K_h^+)$  and then define  $\Omega_{\text{int}} := \bigcup_{K \in \mathcal{T}_h^i} K_{\text{int}}$ . We introduce a  $\delta$ -strip  $S_{\delta} = \{\mathbf{x} : \operatorname{dist}(\mathbf{x}, \Gamma) \leq \delta\}$  and refer readers to Figure 2.2 for illustration. Note that Lemma 5.3 below immediately implies that

(5.1) 
$$\Omega_{\rm int} \subset S_{\delta} \quad \text{for some } \delta \in (0, c_0 h^2].$$

We can control the  $L^2$ -norm on the  $\delta$ -strip by its width.

Lemma 5.1 (see [58]). It holds for any  $z \in H_0^1(\Omega^{\pm})$  that

(5.2) 
$$||z||_{L^2(S_\delta)} \le C\sqrt{\delta}||z||_{H^1(\Omega)}.$$

Next, we recall the  $\mathbf{H}^1(\operatorname{curl};\Omega)$ - and  $\mathbf{H}^1(\operatorname{div};\Omega)$ -extension operators; see Theorem 3.4 and Corollary 3.5 in [47] and Theorem 3.2 in [46]. To simplify the discussion, we shall adopt a general differential operator  $d = \operatorname{curl}$  or  $\operatorname{div}$ .

Theorem 5.2 (see [47, 46]). For d = curl or div, there exist two bounded linear operators

(5.3) 
$$\mathbf{E}_{\mathrm{d}}^{\pm}: \mathbf{H}^{1}(\mathrm{d}; \Omega^{\pm}) \to \mathbf{H}^{1}(\mathrm{d}; \Omega),$$

such that for each  $\mathbf{u} \in \mathbf{H}^1(\mathbf{d}; \Omega^{\pm})$ ,

- 1.  $\mathbf{E}_{d}^{\pm}\mathbf{u} = \mathbf{u}$  a.e. in  $\Omega^{\pm}$ ;
- 2.  $\|\mathbf{E}_{\mathrm{d}}^{\pm}\mathbf{u}\|_{\mathbf{H}^{1}(\mathrm{d};\Omega)} \leq C_{E}\|\mathbf{u}\|_{\mathbf{H}^{1}(\mathrm{d};\Omega^{\pm})}$  with the constant  $C_{E}$  only depending on  $\Omega$ .

With this theorem, we define  $\mathbf{u}_{E,\,\mathrm{d}}^{\pm} = \mathbf{E}_{\,\mathrm{d}}^{\pm}\mathbf{u}^{\pm}$  which are the keys in the analysis. Furthermore, for any subdomain  $D \subset \Omega$ , we employ the following notation for simplicity:

(5.4) 
$$\|\mathbf{u}\|_{E, \mathbf{d}, s, D} = \|\mathbf{u}_{E, \mathbf{d}}^{+}\|_{\mathbf{H}^{s}(\mathbf{d}, D)} + \|\mathbf{u}_{E, \mathbf{d}}^{-}\|_{\mathbf{H}^{s}(\mathbf{d}, D)},$$

and  $\|\mathbf{u}\|_{E,s,D}$  simply denotes the usual Sobolev norm without the curl or div terms. Next, we introduce a patch  $\omega_K$  of each interface element K:

(5.5) 
$$\omega_K = \bigcup \{K' : \partial K' \cap \partial K \neq \emptyset\}.$$

Then, for each  $\omega_K$ , define  $\Gamma^{\omega_K} := \Gamma \cap \omega_K$  and  $\Gamma_h^{\omega_K} := \hat{\Gamma}_h^K \cap \omega_K$ , where  $\hat{\Gamma}_h^K$  is the entire plane containing  $\Gamma_h^K$ . Namely,  $\Gamma_h^{\omega_K}$  is the extension of  $\Gamma_h^K$  to the patch. The following geometric estimates regard the closeness between  $\Gamma^{\omega_K}$  and  $\Gamma_h^{\omega_K}$ .

Lemma 5.3. Suppose  $\Gamma$  is smooth enough such that  $\varphi^{\Gamma}$  is also smooth near the interface, and let the mesh size be sufficiently small. Denote  $\mathbf{n}$  and  $\bar{\mathbf{n}}$  as the normal vectors to  $\Gamma^{\omega_K}$  and  $\Gamma^{\omega_K}_h$  which have the same orientation. For each  $\mathbf{x} \in \Gamma^{\omega_K}_h$ , let  $\mathbf{x}_{\perp}$  be the projection of  $\mathbf{x}$  onto  $\Gamma^{\omega_K}_h$ . Then, for every interface element K and its patch  $\omega_K$ , there holds that

(5.6) 
$$\|\mathbf{x} - \mathbf{x}_{\perp}\| \le c_{\Gamma,1} h_K^2 \quad and \quad \|\mathbf{n} - \bar{\mathbf{n}}\| \le c_{\Gamma,2} h_K.$$

*Proof.* The proof simply follows from the similar argument in [56] by using interpolation on  $\omega_K$ .

**5.2. Special quasi-interpolation operators.** To develop quasi-interpolation for handling the discontinuity of the IFE functions across the interface, by Table 3.1 and (3.1), let us rewrite the functions in  $\mathbf{S}_h^e(K)$  in the following format:

(5.7) 
$$\mathbf{v}_h = \begin{cases} \mathbf{v}_h^+ = \mathbf{a}_h^+ \times (\mathbf{x} - \mathbf{x}_K) + \mathbf{b}_h^+ & \text{in } K_h^+, \\ \mathbf{v}_h^- = \mathcal{C}_K^{\text{curl}}(\mathbf{v}_h^+) := (A_K \mathbf{a}_h^+) \times (\mathbf{x} - \mathbf{x}_K) + (B_K \mathbf{b}_h^+) & \text{in } K_h^-. \end{cases}$$

Similarly, the functions in  $\mathbf{S}_h^f(K)$  can be represented as

(5.8) 
$$\mathbf{v}_h = \begin{cases} \mathbf{v}_h^+ = c_0(\mathbf{x} - \mathbf{x}_K) + \mathbf{a}_h^+ & \text{in } K_h^+, \\ \mathbf{v}_h^- = \mathcal{C}_K^{\text{div}}(\mathbf{v}_h^+) := c_0(\mathbf{x} - \mathbf{x}_K) + (A_K \mathbf{a}_h^+) & \text{in } K_h^-. \end{cases}$$

The operators  $\mathcal{C}_K^{\text{curl}}$  and  $\mathcal{C}_K^{\text{div}}$  can be considered as discrete extensions mapping the polynomial component on the "+" side to the "-" side through the jump conditions. The "-" piece of the IFE functions can be completely determined by the "+" piece.

In addition, we also need an interpolation:  $\mathcal{P}_{\omega_K}^{d}$ :  $\mathbf{H}(\mathbf{d};\omega_K) \to \widetilde{\mathbf{S}}_h(K)$ , where  $\widetilde{\mathbf{S}}_h(K) = \mathcal{N}\mathcal{D}_0(K)$  if  $\mathbf{d} = \text{curl or } \widetilde{\mathbf{S}}_h(K) = \mathcal{R}\mathcal{T}_0(K)$  if  $\mathbf{d} = \text{div such that}$ 

(5.9) 
$$\mathcal{P}_{\omega_K}^{\text{curl}} \mathbf{v} := (\Pi_{\omega_K}^0 \text{ curl } \mathbf{v}) \times (\mathbf{x} - \mathbf{x}_K)/2 + \Pi_{\omega_K}^0 \mathbf{v}, \\ \mathcal{P}_{\omega_K}^{\text{div}} \mathbf{v} := (\Pi_{\omega_K}^0 \text{ div } \mathbf{v})(\mathbf{x} - \mathbf{x}_K)/3 + \Pi_{\omega_K}^0 \mathbf{v},$$

where  $\Pi^0_{\omega_K}$  is simply the projection onto  $[\mathbb{P}_0(\omega_K)]^3$  or  $[\mathbb{P}_0(\omega_K)]$  depending on the dimension. Note that  $\mathcal{P}^{\mathrm{d}}_{\omega_K}$  will be applied only to each Sobolev extension  $\mathbf{u}_{E,\,\mathrm{d}}^{\pm}$  which are smooth functions involving no discontinuity. The quasi-interpolation has the commutative diagram property:

(5.10) 
$$\mathbf{d} \circ \mathcal{P}_{\omega_K}^{\mathbf{d}} = \Pi_{\omega_K}^0 \circ \mathbf{d},$$

which is illustrated in the diagram in Figure 5.1.

Now, with  $\mathcal{C}_K^d$  and  $\mathcal{P}_{\omega_K}^d$ , we define the quasi-interpolation  $J_K^d: \mathbf{H}(d;K) \to \mathbf{S}_h(K)$  where  $\mathbf{S}_h(K) = \mathbf{S}_h^e(K)$  if  $d = \text{curl or } \mathbf{S}_h(K) = \mathbf{S}_h^f(K)$  if d = div, such that

$$J_K^{\mathbf{d}}\mathbf{u} = \begin{cases} J_K^{\mathbf{d},+}\mathbf{u} = \mathcal{P}_{\omega_K}^{\mathbf{d}}\mathbf{u}_{E,\,\mathbf{d}}^+ & \text{in } K_h^+, \\ J_K^{\mathbf{d},-}\mathbf{u} = \mathcal{C}_K^{\mathbf{d}}(\mathcal{P}_{\omega_K}^{\mathbf{d}}\mathbf{u}_{E,\,\mathbf{d}}^+) & \text{in } K_h^-. \end{cases}$$

Remark 5.4. Let us briefly explain the motivation for the quasi-interpolation in (5.11) by establishing a diagram in Figure 5.2. Suppose  $\mathcal{P}_{\omega_K}^{\mathrm{d}}(\mathbf{u}_{E,\,\mathrm{d}}^+)$  has sufficient approximation to  $\mathbf{u}_{E,\,\mathrm{d}}^+$ . Then, its discrete extension  $\mathcal{C}_K^{\mathrm{d}}(\mathcal{P}_{\omega_K}^{\mathrm{d}}\mathbf{u}_{E,\,\mathrm{d}}^+)$  is also expected to be a good approximation to  $\mathbf{u}_{E,\,\mathrm{d}}^-$ . So the quasi-interpolation  $J_K^{\mathrm{d}}$  behaves close to a Hermitian-type interpolation. The quasi-interpolation plays an important role in our analysis. In fact, roughly speaking, the robustness of the approximation capabilities of the IFE spaces with respect to irregular subelements is attributed to the fact that  $\mathcal{C}_K^{\mathrm{d}}$  can stably extend the polynomials from one subelement to another in the sense of  $\|A_K\|_2 \lesssim 1$  and  $\|B_K\|_2 \lesssim 1$ .

Remark 5.4 suggests the following decomposition:

$$(5.12) \qquad \mathbf{u}^{-} - J_{K}^{\mathrm{d},-}\mathbf{u} = (\mathbf{u}^{-} - \mathcal{P}_{\omega_{K}}^{\mathrm{d}}\mathbf{u}_{E,d}^{-}) + (\mathcal{P}_{\omega_{K}}^{\mathrm{d}}\mathbf{u}_{E,d}^{-} - J_{K}^{\mathrm{d},-}\mathbf{u}) := \boldsymbol{\xi}_{\mathbf{u}} + \boldsymbol{\eta}_{\mathbf{u}}.$$

Now we estimate each term above. Let us begin with  $\xi_{\mathbf{u}}$  in the following lemma.

LEMMA 5.5. For  $\mathbf{w} \in \mathbf{H}^1(\mathbf{d}; \omega_K)$ , there holds

(5.13) 
$$\|\mathbf{w} - \mathcal{P}_{\omega_K}^{d} \mathbf{w}\|_{\mathbf{H}(\mathbf{d};\omega_K)} \lesssim h_K \|\mathbf{w}\|_{\mathbf{H}^1(\mathbf{d};\omega_K)}.$$

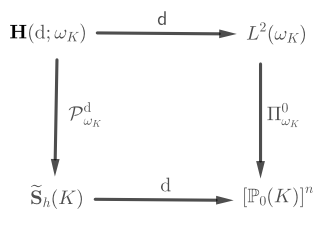


Fig. 5.1. The commutative diagram for  $\mathcal{P}_{\omega_K}^d$ .

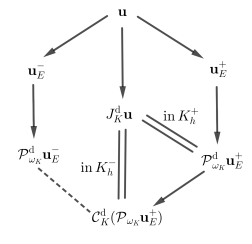


Fig. 5.2. The diagram for interpolation.

*Proof.* The estimate for the  $L^2$ -norm directly follows from the approximation result of  $\Pi^0_{\omega_K}$  and  $\|\mathbf{x} - \mathbf{x}_K\| \lesssim h_K$  for  $\mathbf{x} \in \omega_K$ . The estimate for the d-seminorm additionally follows from (5.10).

The estimate of  $\eta_{11}$  is included in the following lemma.

LEMMA 5.6. For  $\mathbf{u} \in \mathbf{H}^1(\alpha, \beta, \text{curl}; \Omega)$  with d = curl and  $\mathbf{u} \in \mathbf{H}^1(\alpha, \text{div}; \Omega)$  with d = div,

(5.14) 
$$\|\mathcal{P}_{\omega_{K}}^{d}\mathbf{u}_{E,d}^{-} - \mathcal{C}_{K}^{d}(\mathcal{P}_{\omega_{K}}^{d}\mathbf{u}_{E,d}^{+})\|_{\mathbf{H}(d;\omega_{K})} \lesssim h_{K}\|\mathbf{u}\|_{E,d,1,\omega_{K}}.$$

*Proof.* As the argument is lengthy and similar to the 2D case [41], for the sake of completeness, we put it in section SM3 of the supplementary materials.  $\Box$ 

Now, we are ready to estimate  $J_K^d$ .

LEMMA 5.7. For  $\mathbf{u} \in \mathbf{H}^1(\alpha, \beta, \text{curl}; \Omega)$  or  $\mathbf{u} \in \mathbf{H}^1(\alpha, \text{div}; \Omega)$ , there holds

(5.15) 
$$\|\mathbf{u}_{E, d}^{\pm} - J_{K}^{d, \pm} \mathbf{u}\|_{\mathbf{H}(d; \omega_{K})} \lesssim h_{K} \|\mathbf{u}\|_{E, d, 1, \omega_{K}}.$$

*Proof.* The result immediately follows from the definition (5.11) and applying the triangular inequality to (5.12) together with Lemmas 5.5 and 5.6.

**5.3. Face and edge interpolation estimates.** Lemma 5.7 only gives the local approximation capabilities. We then estimate the global spaces through the edge and face interpolations. Let us first present the following estimates for the bounds of the face and edge shape functions for which the proof immediately follows from Lemmas 3.2 and 3.3, respectively.

Lemma 5.8. Given a trirectangular tetrahedral or regular tetrahedral interface element K, it holds that

(5.16) 
$$\|\phi_i^f\|_{L^{\infty}(K)} \lesssim h_K^{-2} \text{ and } \|\operatorname{div}\phi_i^f\|_{L^{\infty}(K)} \lesssim h_K^{-3}, \quad i = 1, 2, \dots, 4,$$

(5.17) 
$$\|\phi_i^e\|_{L^{\infty}(K)} \lesssim h_K^{-1} \text{ and } \|\operatorname{curl} \phi_i^e\|_{L^{\infty}(K)} \lesssim h_K^{-2}, \quad i = 1, 2, \dots, 6.$$

Let us briefly explain the idea of interpolation estimation. The key is to employ  $J_K^d$  as the bridge. Let  $I_h$  be  $I_h^e$  if d = curl or  $I_h^f$  if d = div. Then, the following triangular inequality holds:

(5.18) 
$$\|\mathbf{u} - I_h \mathbf{u}\|_{L^2(K)} \le \|\mathbf{u} - J_K^{d} \mathbf{u}\|_{L^2(K)} + \|J_K^{d} \mathbf{u} - I_h \mathbf{u}\|_{L^2(K)}.$$

For the first term in the right-hand side of (5.18), Lemma 5.7 almost gives the desired result, but special attention must be paid to the different partitions of  $\mathbf{u}$  and  $J_K \mathbf{u}$  which are defined with  $\Gamma$  and  $\Gamma_h^K$ , respectively.

LEMMA 5.9. For  $\mathbf{u} \in \mathbf{H}^1(\alpha, \beta, \text{curl}; \Omega)$  or  $\mathbf{u} \in \mathbf{H}^1(\alpha, \text{div}; \Omega)$ , there holds

(5.19) 
$$\sum_{K \in \mathcal{T}^{i}} \|\mathbf{u} - J_{K}^{d}\mathbf{u}\|_{L^{2}(K)} \lesssim h(\|\mathbf{u}\|_{\mathbf{H}^{1}(d;\Omega^{-})} + \|\mathbf{u}\|_{\mathbf{H}^{1}(d;\Omega^{+})}).$$

*Proof.* On each interface element K, we have

where the estimate of the first term is readily given by Lemma 5.7. Summing (5.20) over all the interface elements and applying (5.1), Lemma 5.1, as well as Theorem 5.2, we have (5.19).

Next, we turn to the term  $||J_K^{\mathbf{d}}\mathbf{u} - I_h\mathbf{u}||_{L^2(K)}$  in (5.18). We first prepare the following estimate.

LEMMA 5.10. For  $\mathbf{u} \in \mathbf{H}^1(\alpha, \beta, \operatorname{curl}; \Omega)$  or  $\mathbf{u} \in \mathbf{H}^1(\alpha, \operatorname{div}; \Omega)$ , given a  $\delta$ -strip with  $\delta \lesssim h^2$ , there holds

(5.21) 
$$\sum_{K \in \mathcal{T}_h^i} \|J_K^{\mathbf{d},\pm} \mathbf{u}\|_{L^2(S_\delta \cap \omega_K)} \lesssim h \|\mathbf{u}\|_{\mathbf{H}^1(\mathbf{d};\Omega^+)}.$$

*Proof.* For the "+" component, with  $|S_{\delta} \cap \omega_K| \lesssim h_K^4$  and  $\|\mathbf{x} - \mathbf{x}_K\|_{L^2(S_{\delta} \cap \omega_K)} \lesssim h_K^3$ , we have

where we have used the boundedness property of the projection  $\Pi^0_{\omega_K}$  in the last inequality. Then, the desired estimate follows from summing (5.22) over all the interface elements, using the finite overlapping of  $\omega_K$ , and applying the  $\delta$ -strip argument from Lemma 5.1 with  $\delta \simeq h_K$  as well as Theorem 5.2. For the "-" side, by (3.2), we have the boundedness  $||A_K|| \lesssim 1$  and  $||B_K|| \lesssim 1$ . Therefore, it also holds that

for which the estimate is the same as (5.22).

Now, with the estimate in Lemma 5.9, we proceed to show the second term in (5.18) and split the discussion for the edge and face elements.

- **5.3.1. Face interpolation.** Let us first consider the face interpolation and fix d = div. We need an assumption to handle the mismatching portion of faces:
  - (A1) For each interface element  $K \in \mathcal{T}_h^i$  and each face of F, define  $\tilde{F} = F \cap K_{\text{int}}$ . Assume that there exists a  $\delta$ -strip  $S_{\delta_1}$  with  $\delta_1 \simeq O(h^2)$  such that for every  $K \in \mathcal{T}_h^i$ , there is a pyramid  $P_{\tilde{F}} \subset \omega_K \cap S_{\delta_1}$  with  $\tilde{F}$  as its base satisfying that the height  $l_{\tilde{F}}$  of  $P_{\tilde{F}}$  supporting  $\tilde{F}$  is  $\mathcal{O}(h_K)$ .

We refer readers to Figure SM4.2 in the supplementary materials for an illustration of  $(\mathbf{A2})$ .

THEOREM 5.11. For  $\mathbf{u} \in \mathbf{H}^1(\alpha, \operatorname{div}; \Omega)$ , under assumption (A1), there holds

(5.24) 
$$\|\mathbf{u} - I_h^f \mathbf{u}\|_{L^2(\Omega)} \lesssim h(\|\mathbf{u}\|_{\mathbf{H}^1(\operatorname{div};\Omega^-)} + \|\mathbf{u}\|_{\mathbf{H}^1(\operatorname{div};\Omega^+)}).$$

*Proof.* We only consider interface elements. Given  $K \in \mathcal{T}_h^i$ , by (5.18) and Lemma 5.9, it remains to estimate  $\|J_K^{\mathbf{d}}\mathbf{u} - I_h^f\mathbf{u}\|_{L^2(K)}$ . We need an auxiliary function  $\mathbf{w}$  such that  $\mathbf{w}^{\pm} = J_K^{\mathbf{d},\pm}\mathbf{u} - \mathbf{u}_{E,\,\mathbf{d}}^{\pm}$  in  $K^{\pm}$ , i.e., it is partitioned with  $\Gamma$ . Note that  $\mathbf{w}$  is slightly different from  $J_K^{\mathbf{d}}\mathbf{u} - \mathbf{u}$  as  $J_K^{\mathbf{d}}\mathbf{u}$  is defined with  $\Gamma_h^K$ , and thus this difference is only on  $K_{\mathrm{int}}$ . To control the mismatch, by assumption (A1) and the trace inequality for polynomials [74], we have

$$(5.25) ||J_K^{\mathbf{d},+}\mathbf{u} - J_K^{\mathbf{d},-}\mathbf{u}||_{L^2(\tilde{F})} \lesssim h_K^{-1/2} (||J_K^{\mathbf{d},+}\mathbf{u}||_{L^2(S_{\delta_1 \cap \omega_K})} + ||J_K^{\mathbf{d},-}\mathbf{u}||_{L^2(S_{\delta_1 \cap \omega_K})}).$$

Note that each component of  $\mathbf{w}^{\pm}$  can be naturally extended to the whole element and whole patch. As  $\mathbf{w}^{\pm} \in \mathbf{H}^{1/2}(F)$  for each face of F, by the trace inequality and Lemma 5.7 we have

(5.26) 
$$\|\mathbf{w}^{\pm}\|_{L^{2}(F^{\pm})} \lesssim \|\mathbf{w}^{\pm}\|_{L^{2}(F)} \\ \lesssim h_{K}^{-1/2} \|\mathbf{w}\|_{L^{2}(K)} + h_{K}^{1/2} \|\mathbf{w}|_{H^{1}(K)} \lesssim h_{K}^{1/2} \|\mathbf{u}\|_{E, \operatorname{div}, 1, \omega_{K}}.$$

Now, by the definition of the face interpolation, we obtain

$$\begin{split} \|J_{K}^{\mathbf{d}}\mathbf{u} - I_{h}^{f}\mathbf{u}\|_{L^{2}(K)} &= \|I_{h}^{f}(J_{K}^{\mathbf{d}}\mathbf{u} - \mathbf{u})\|_{L^{2}(K)} \\ &\lesssim \|\boldsymbol{\phi}_{i}^{f}\|_{L^{2}(K)} \left[ \sum_{i=1}^{4} |F_{i}|^{1/2} (\|\mathbf{w}^{+} \cdot \mathbf{n}\|_{L^{2}(F_{i})} + \|\mathbf{w}^{-} \cdot \mathbf{n}\|_{L^{2}(F_{i})}) \right. \\ &+ |\tilde{F}_{i}|^{1/2} \|J_{K}^{\mathbf{d},+}\mathbf{u} - J_{K}^{\mathbf{d},-}\mathbf{u}\|_{L^{2}(\tilde{F}_{i})} \right] \\ &\lesssim h_{K} \|\mathbf{u}\|_{E, \operatorname{div}, 1, \omega_{K}} + (\|J_{K}^{\mathbf{d},+}\mathbf{u}\|_{L^{2}(S_{\delta_{1} \cap \omega_{K}})} + \|J_{K}^{\mathbf{d},-}\mathbf{u}\|_{L^{2}(S_{\delta_{1} \cap \omega_{K}})}), \end{split}$$

where we have used (5.25), (5.26), and Lemma 5.8. Summing the estimates above over all the elements, using the finite overlapping property of  $\omega_K$ , and applying Lemma 5.9 and Theorem 5.2 yields the desired result.

The estimate of  $\operatorname{div}(\mathbf{u} - I_h^f \mathbf{u})$  is trivial as  $\operatorname{div} I_h^f \mathbf{u} = \Pi_0 \operatorname{div} \mathbf{u}$  by Lemma 3.7. At last, we present the following estimate.

THEOREM 5.12. For  $\mathbf{u} \in \mathbf{H}^1(\alpha, \operatorname{div}; \Omega)$ , there holds

(5.27) 
$$\|\operatorname{div}(\mathbf{u} - I_h^f \mathbf{u})\|_{L^2(\Omega)} \lesssim h(\|\mathbf{u}\|_{\mathbf{H}^1(\operatorname{div};\Omega^-)} + \|\mathbf{u}\|_{\mathbf{H}^1(\operatorname{div};\Omega^+)}).$$

- **5.3.2. Edge interpolation.** Next, we proceed to estimate the approximation capabilities of  $\mathbf{S}_h^e$  through  $I_h^e$ . We need a similar assumption to (A1).
- (A2) For each interface element  $K \in \mathcal{T}_h^i$  and each edge e, define  $\tilde{e} = e \cap K_{\text{int}}$ , i.e., the portion of the edge contained in the mismatching region  $K_{\text{int}}$ . Assume that there exists a  $\delta$ -strip  $S_{\delta_2}$  with  $\delta_2 \simeq O(h^2)$  such that for every  $K \in \mathcal{T}_h^i$ , there is a tetrahedron  $T_{\tilde{e}} \subset \omega_K \cap S_{\delta_2}$  with  $\tilde{e}$  as one of its edges satisfying  $|T_{\tilde{e}}| \gtrsim |\tilde{e}|^2 h_K$ .

Also see Figure SM4.2 in the supplementary materials for illustration. In the following discussion, we fix d = curl.

THEOREM 5.13. For  $\mathbf{u} \in \mathbf{H}^1(\alpha, \beta, \text{curl}; \Omega)$ , under assumption (A3), there holds

(5.28) 
$$\|\mathbf{u} - I_h^e \mathbf{u}\|_{L^2(\Omega)} \lesssim h(\|\mathbf{u}\|_{\mathbf{H}^1(\operatorname{curl};\Omega^-)} + \|\mathbf{u}\|_{\mathbf{H}^1(\operatorname{curl};\Omega^+)}).$$

*Proof.* We still only consider interface elements. Similar to the argument of Theorem 5.11, we only need to estimate  $\|J_K^d \mathbf{u} - I_h^e \mathbf{u}\|_{L^2(K)}$ . Define the same auxiliary function  $\mathbf{w}$  partitioned with  $\Gamma$ :  $\mathbf{w}^{\pm} = J_K^{\mathrm{d},\pm} \mathbf{u} - \mathbf{u}_{E,\mathrm{d}}^{\pm}$  in  $K^{\pm}$ . Let us estimate  $J_K^{\mathrm{d},+} \mathbf{u} - J_K^{\mathrm{d},-} \mathbf{u}$  on the small subedge  $\tilde{e}$ . By assumption (A3) and the trace inequality for polynomials [74], we obtain

$$\|J_K^{\mathrm{d},+}\mathbf{u} - J_K^{\mathrm{d},-}\mathbf{u}\|_{L^2(\tilde{e})} \lesssim h_K^{-1/2} |\tilde{e}|^{-1/2} (\|J_K^{\mathrm{d},+}\mathbf{u}\|_{L^2(S_{\delta_2 \cap \omega_K})} + \|J_K^{\mathrm{d},-}\mathbf{u}\|_{L^2(S_{\delta_2 \cap \omega_K})}).$$

In addition, as  $\mathbf{u}_{E,\,\mathbf{d}}^{\pm} \in \mathbf{H}^{1}(\mathrm{curl};\Omega)$ , the first moment  $\int_{e} \mathbf{u}_{E,\,\mathbf{d}}^{\pm} \cdot \mathbf{t} \, \mathrm{d}s$  is well defined on each edge e. Furthermore, we have  $\mathbf{u}_{E,\,\mathbf{d}}^{\pm} \in \mathbf{H}^{1/2}(F) \cap \mathbf{H}(\mathrm{rot};F)$  on each face F. Thus, by Lemma 4.4 in [8] and the trace inequality, we obtain for each face F of K and any edge e that

$$(5.30) \|\mathbf{w}^{\pm} \cdot \mathbf{t}\|_{L^{1}(e^{\pm})} \lesssim \|\mathbf{w}^{\pm} \cdot \mathbf{t}\|_{L^{1}(e)}$$

$$\lesssim \|\mathbf{w}^{\pm}\|_{L^{2}(F)} + h_{F}^{1/2} \|\mathbf{w}^{\pm}\|_{H^{1/2}(F)} + h_{F} \|\operatorname{rot}_{F} \mathbf{w}^{\pm}\|_{L^{2}(F)}$$

$$\lesssim h_{K}^{-1/2} \|\mathbf{w}^{\pm}\|_{L^{2}(K)} + h_{K}^{1/2} \|\mathbf{w}^{\pm}\|_{H^{1}(K)}$$

$$+ h_{K}^{1/2} \|\operatorname{curl} \mathbf{w}^{\pm}\|_{L^{2}(K)} + h_{K}^{3/2} \|\operatorname{curl} \mathbf{w}^{\pm}\|_{H^{1}(K)} \lesssim h_{K}^{1/2} \|\mathbf{u}\|_{E,\operatorname{curl},1,\omega_{K}},$$

where we have used Lemma 5.7 in the fourth inequality with the following estimates:

$$\|\mathbf{w}^{\pm}\|_{H^{1}(K)} \lesssim \|\mathbf{u}_{E, \, \mathbf{d}}^{\pm}\|_{H^{1}(K)} + \|\operatorname{curl} J_{K}^{\mathbf{d}, \pm} \mathbf{u}\|_{L^{2}(K)} \lesssim \|\mathbf{u}\|_{E, \operatorname{curl}, 1, \omega_{K}}, \\ \|\operatorname{curl} \mathbf{w}^{\pm}\|_{H^{1}(K)} \lesssim \|\operatorname{curl} \mathbf{u}_{E, \, \mathbf{d}}^{\pm}\|_{H^{1}(K)} \lesssim \|\mathbf{u}\|_{E, \operatorname{curl}, 1, \omega_{K}}.$$

Then, it follows from the definition of  $J_K^d$  together with (5.29), (5.30), and Lemma 5.8 that

(5.31)

$$\begin{split} \|J_{K}^{\mathbf{d}}\mathbf{u} - I_{h}^{e}\mathbf{u}\|_{L^{2}(K)} &= \|I_{h}^{e}(J_{K}^{\mathbf{d}}\mathbf{u} - \mathbf{u})\|_{L^{2}(K)} \\ &\leq \left(\sum_{i=1}^{6} \int_{e_{i}} |\mathbf{w} \cdot \mathbf{t}| \, \mathrm{d}s + |\tilde{e}_{i}|^{1/2} \|J_{K}^{\mathbf{d},+}\mathbf{u} - J_{K}^{\mathbf{d},-}\mathbf{u}\|_{L^{2}(\tilde{e}_{i})}\right) \|\boldsymbol{\phi}_{i}^{e}\|_{L^{2}(K)} \\ &\lesssim h_{K} \|\mathbf{u}\|_{E, \mathrm{curl}, 1, \omega_{K}} + (\|J_{K}^{\mathbf{d},+}\mathbf{u}\|_{L^{2}(S_{\delta_{2} \cap \omega_{K}})} + \|J_{K}^{\mathbf{d},-}\mathbf{u}\|_{L^{2}(S_{\delta_{2} \cap \omega_{K}})}). \end{split}$$

Summing (5.31) over all the interface elements, using the finite overlapping property of  $\omega_K$ , and applying Lemma 5.9 and Theorem 5.2 leads to the desired estimate.

Remark 5.14. One key in the proof is to use assumption (A3) with the trace inequality for polynomials to control  $J_K^{\mathbf{d},\pm}\mathbf{u}$  on edges. If this is done for  $\mathbf{u}_{E,\mathbf{d}}^{\pm}$ , one must be careful about bounding  $\|\mathbf{u}_{E,\mathbf{d}}\|_{L^2(\tilde{e})}$  since it may not be well-defined for  $\mathbf{u} \in \mathbf{H}^1(\omega_K)$ .

Finally, as  $\operatorname{curl} I_h^e \mathbf{u} = I_h^f \operatorname{curl} \mathbf{u}$ , Theorem 5.11 immediately yields the estimate for  $\operatorname{curl}(\mathbf{u} - I_h^e \mathbf{u})$ ,  $\mathbf{u} \in \mathbf{H}^1(\alpha, \beta, \operatorname{curl}; \Omega)$ .

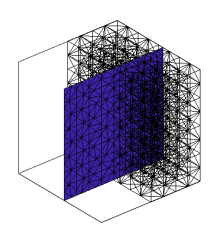
THEOREM 5.15. Under assumption (A3), for  $\mathbf{u} \in \mathbf{H}^1(\alpha, \beta, \text{curl}; \Omega)$ , there holds

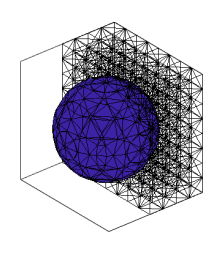
(5.32) 
$$\|\operatorname{curl}(\mathbf{u} - I_h^e \mathbf{u})\|_{L^2(\Omega)} \lesssim h(\|\mathbf{u}\|_{\mathbf{H}^1(\operatorname{curl};\Omega^-)} + \|\mathbf{u}\|_{\mathbf{H}^1(\operatorname{curl};\Omega^+)}).$$

- **6. Numerical experiments.** In this section, we present a group of numerical experiments to demonstrate the performance of the proposed method. We fix the cubic domain to be  $\Omega = (-1,1)^3$  but with varying interface shapes. The background Cartesian mesh is generated by  $N^3$  uniform cubes, each of which is partitioned into tetrahedra. In [41] for the 2D case, numerical experiments were provided to show that the standard Galerkin methods with or without penalties do not converge. Similar behavior can also be observed in the 3D case, and here we omit their comparison.
- **6.1. Test 1 (stability).** In the first test, we study the numerical stability of the method with respect to the mesh size and the interface location. We first provide a group of numerical estimates for the quantity  $\eta_s$  in (4.10) indicating a lower bound of the *inf-sup* constant. We consider the spherical interface shape shown in the middle plot of Figure 6.1 for the three groups of parameters:

(6.1) 
$$\left(\frac{\max(\beta^+, \beta^-)}{\min(\beta^+, \beta^-)}, \frac{\max(\alpha^+, \alpha^-)}{\min(\alpha^+, \alpha^-)}\right) = (200, 100), (200, 1000), (2000, 1000),$$

where the minimal values are always set as 1; see the detailed parameter illustration in the right corner of plots in Figure 6.2. Then, we consider a sequence of meshes with N=10,20,30,40,50,60,70. We plot the values of  $\eta_s$  in Figure 6.2. Here, the computational results for the first two groups of parameters are presented in the first two plots, but for the third group, we separate the parameter  $(\beta^+, \alpha^-) = (2000, 100)$  in a single plot to show more details. Overall, we can see that  $\eta_s$  is bounded below. More specifically, we can make the following numerical observations:





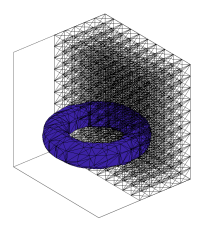
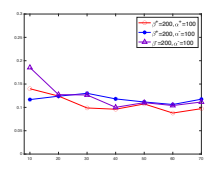
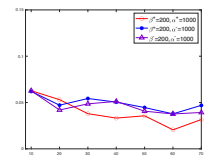
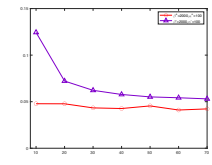


Fig. 6.1. A flat interface (left), a spherical interface (middle), and a torus interface (right).







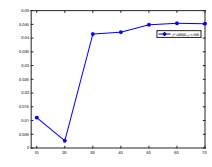


Fig. 6.2. Estimates of  $\eta_s$  for various  $\alpha$ ,  $\beta$  and mesh sizes.

Table 6.1 Condition numbers for the flat interface with various  $\epsilon$ .

$\epsilon$	$10^{-1}$	$10^{-2}$	$10^{-3}$	$10^{-4}$	$10^{-5}$	$10^{-6}$
$\operatorname{cond}(\mathbf{B}^{PG})$	88267	83052	78834	84570	78253	81324

- $\eta_s$  slightly decreases at the beginning, and then the curve proceeds to be flat as the mesh becomes finer.
- $\eta_s$  highly depends on the contrast of the parameters, and the larger contrast leads to smaller  $\eta_s$ . Particularly, the values decrease from the first to the third group of parameters.
- For the third group where the parameters have the ratio (2000, 100), when  $(\alpha^-, \beta^+) = (100, 2000)$ ,  $\eta_s \approx 2.6 \times 10^{-3}$  for the mesh N = 20, which is indeed close to zero. But it turns back to around 0.05 for finer meshes.

These observations are consistent with the analysis in two dimensions (cf. [41]) that the *inf-sup* condition only holds for sufficiently small mesh size.

Next, we test the condition number of  $\mathbf{B}^{PG}$  with respect to various interface locations. Let us fix mesh size N=10 and choose  $(\alpha^-,\alpha^+)=(1,100), (\beta^-,\beta^+)=(1,200)$ . Consider a flat interface  $(\mathbf{x}-\mathbf{x}_0)\cdot\mathbf{n}=0$  passing through  $\mathbf{x}_0=[\epsilon,0,0]$  with  $\epsilon=10^{-j},\ j=1,2,\ldots,6$  and the normal vector  $\mathbf{n}=[1,0,0]^{\top}$  such that the interface gradually moves to one face/edge of interface elements. Thus, small subelements exist for every interface element. The condition numbers, estimated through the condest command in MATLAB, are shown in Table 6.1 for various  $\epsilon$ . In fact, as the interface element shrinks to a noninterface element, the IFE functions will converge to standard FE functions, which is "good" for computation.

**6.2. Test 2 (optimal convergence).** In the second test, we investigate the optimal convergence rates with respect to the mesh size and speed of the fast solver. Consider a spherical interface with a radius  $r_1$  shown in the left plot of Figure 6.1. We still employ (1.3) as the model equation and use the benchmark example from [41] in which the analytical solution is given by

(6.2) 
$$\mathbf{u} = \begin{cases} \frac{1}{\beta^{-}} \mathbf{x} + \frac{1}{\alpha^{-}} n_{1} R_{1}(\mathbf{x}) [(x_{2} - x_{3}), (x_{3} - x_{1}), (x_{1} - x_{2})]^{\top} & \text{in } \Omega^{-}, \\ \frac{1}{\beta^{+}} \mathbf{x} + \frac{1}{\alpha^{+}} n_{2} R_{1}(\mathbf{x}) R_{2}(\mathbf{x}) [(x_{2} - x_{3}), (x_{3} - x_{1}), (x_{1} - x_{2})]^{\top} & \text{in } \Omega^{+}, \end{cases}$$

where  $\mathbf{x} = [x_1, x_2, x_3]^{\top}$ ,  $R_1(\mathbf{x}) = r_1^2 - ||\mathbf{x}||^2$ ,  $R_2(\mathbf{x}) = r_2^2 - ||\mathbf{x}||^2$ , and  $n_1 = n_2(r_2^2 - r_1^2)$ . We let  $(\alpha^-, \alpha^+) = (\beta^-, \beta^+) = (1, 100)$  and (1, 1000), and denote  $\rho = \alpha^+/\alpha^- = \beta^+/\beta^-$ . We present the numerical results for  $N = 10, \ldots, 70$  in Figure 6.3 which clearly show the optimal convergence rates.

To solve the linear system, we employ the HX preconditioner described in section 4.2 with both GMRES and CG iteration strategies. It involves a direct solver on a smaller matrix for which the size depends on the expanding width l, i.e., the size of  $\mathbf{B}_{i}^{(2,2)}$  in (4.5). But the block diagonal smoother in (4.6) can help in greatly reducing the iteration steps for convergence, and consequently significantly reduce the computational time. In fact, as l is small, in practice we store the LU factorization of  $\mathbf{B}_{r}^{(2,2)}$  to avoid repeatedly computing the inverse. In Table 6.2, we present both the number of iterations and computational time for GMRES. It is noteworthy that the preconditioning strategy even works for a CG method which in general does not converge for non-SPD matrices. The results are presented in Table 6.3, and we can observe that the CG method must need l=1 at least for convergence. But once the block diagonal smoother in (4.6) is used, the CG method has better performance than GMRES. We may refer to our detailed discussions in section 4.2 and point out again the important fact that the majority portion of  $\mathbf{B}^{PG}$  is symmetric, and the problematic portion is only around the interface which can be well handled by the direct inverse  $(\mathbf{B}_{l}^{(2,2)})^{-1}$ . Overall, for both methods, we observe that the expanding width l depends on the contrast  $\rho$ . For a larger contrast, there needs to be a relatively larger l to ensure fast convergence. With an appropriately chosen expanding

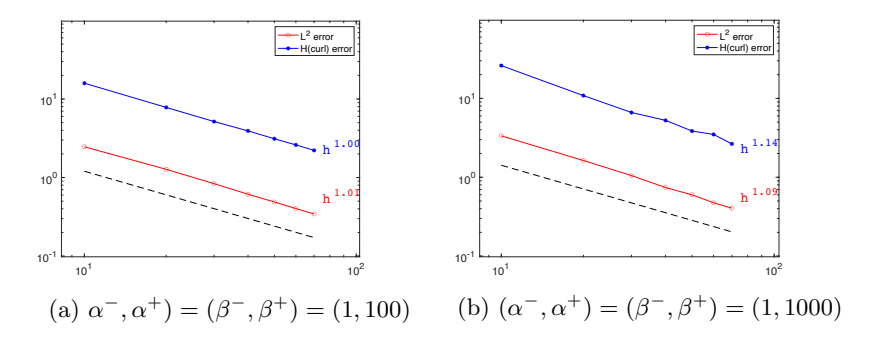


FIG. 6.3. Errors for Test 2 where the dashed line is the reference line indicating  $\mathcal{O}(h)$ . Left:  $(\alpha^-, \alpha^+) = (\beta^-, \beta^+) = (1,100)$ . Right:  $(\alpha^-, \alpha^+) = (\beta^-, \beta^+) = (1,1000)$ .

Table 6.2
Iteration numbers and computational time for the GMRES solver.

# DoFs	7930	59660	197190	462520	897650	1544580	2445310
$\rho = 100, \ l = 0$	63(2.6s)	66(14s)	66(29s)	67(51s)	68(108s)	68(191s)	68(283s)
$\rho = 100, \ l = 1$	35(2.1s)	40(7.9s)	39(14s)	40(28s)	40(56s)	38(100s)	41(147s)
$\rho = 1000, \ l = 0$	212(8.9s)	244(60s)	263(117s)	223(185s)	246(404s)	272(817s)	234(1017s)
$\rho = 1000, \ l = 1$	55(8.4s)	63(13.7s)	76(33s)	48(35s)	46(70s)	52(143s)	54(243s)
$\rho = 1000, \ l = 2$	42(1.9s)	47(11.2s)	46(21s)	52(39s)	46(83s)	51(144s)	51(209s)
$\rho = 1000, \ l = 3$	41(2.2s)	39(11s)	42(20s)	39(40s)	42(75s)	42(135s)	42(191s)

Table 6.3
Iteration numbers and computational time for the CG solver.

# DoFs	7930	59660	197190	462520	897650	1544580	2445310
$\rho = 100, \ l = 0$	_	84(18s)	78(29s)	-	-	_	_
$\rho = 100, \ l = 1$	37(1.6s)	39(9.8s)	40(18s)	41(30s)	42(56s)	42(99s)	43(140s)
$\rho = 100, \ l = 2$	36(1.3s)	39(10s)	41(17s)	42(32s)	42(66s)	42(110s)	42(170s)
$\rho = 1000, \ l = 0$	_	_	_	_	_	_	_
$\rho = 1000, \ l = 1$	40(1.4s)	42(17s)	42(30s)	42(30s)	43(59s)	45(100s)	43(140s)
$\rho = 1000, \ l = 2$	37(1.4s)	39(8.4s)	40(18s)	41(29s)	42(61s)	44(110s)	42(150s)

width, the algorithm converges in a small number of iterations, which indeed takes significantly less computational time.

**6.3. Test 3 (application to a time-domain Maxwell equation).** In this test, we consider the scattering problem modeled by (1.2) in a time domain [0, T]. We partition it into M subintervals:  $t_0 = 0 < t_1 < t_2 < \cdots < t_M = T$  with equal length  $\tau = T/M$ . We then apply the implicit time-discretization method introduced in [30] which reads as

$$(6.3) \quad (\epsilon \partial_{\tau}^{2} \mathbf{u}_{h}^{n}, \mathbf{v}_{h})_{\Omega} + (\sigma \partial_{\tau} \mathbf{u}_{h}^{n}, \mathbf{v}_{h})_{\Omega} + (\mu^{-1} \operatorname{curl} \mathbf{u}_{h}^{n}, \operatorname{curl} \mathbf{v}_{h})_{\Omega} = (\mathbf{J}_{t}, \mathbf{v}_{h})_{\Omega} \quad \forall \mathbf{v}_{h} \in \mathbf{S}_{h}^{e},$$

where, for  $n \geq 2$ ,  $\partial_{\tau} \mathbf{u}_{h}^{n} = (\mathbf{u}_{h}^{n} - \mathbf{u}_{h}^{n-1})/\tau$  and  $\partial_{\tau}^{2} \mathbf{u}_{h}^{n} = (\partial_{\tau} \mathbf{u}_{h}^{n} - \partial_{\tau} \mathbf{u}_{h}^{n-1})/\tau$ . Then, at each time step it can be discretized by the PG-IFE scheme with the parameters  $\alpha = \mu^{-1}$  and  $\beta = \epsilon \tau^{-2} + \sigma \tau^{-1}$  and solved with the proposed fast solver. Here, we consider a simulation problem of electromagnetic waves propagating through a torus where the analytical solution is difficult, if not impossible, to derive, but instead we compare the results of the IFE method and the standard FE method on fitted meshes.

The torus interface shown in the right plot of Figure 6.1 is described by a level-set signed-distance function:

$$\gamma(\mathbf{x}) = (\sqrt{(x_1 - z_1)^2 + (x_2 - z_2)^2} - r_2)^2 + (x_3 - z_3)^2 - r_1^2,$$

where  $z_1=z_2=0$ ,  $z_3=-0.3$  and  $r_1=0.2$ ,  $r_2=\pi/5$ . We further set the medium parameters as  $\epsilon^+=0.05$ ,  $\epsilon^-=2\epsilon^+$ ,  $\sigma^+=0.1$ ,  $\sigma^-=1$ , and  $\mu^+=4\pi$ ,  $\mu^-=3\mu^+$ . Initially, we impose a Gaussian pulse

(6.4) 
$$\mathbf{u} = \exp(-b(a(x_1 - z_0) - \omega t)^2)[0, 1, 0]^{\top},$$

where  $a = \omega \sqrt{\epsilon^+ \mu^+}$  modeling the speed of the electromagnetic wave. In addition, the boundary condition is set to match (6.4) except on the faces at  $\mathbf{x} = -1, 1$  where it is set as **0**. Set the source as  $\mathbf{J} = \mathbf{0}$ , let the time domain be [0, 1.5], and let the step size be  $\tau = 1.5/128$ . The IFE method is computed on an unfitted mesh containing 1,872,064 DoFs, while the FE method is computed on a fitted mesh containing 2,002,947 DoFs.

To compare the simulation results, we first plot the evolution of the  $x_2$  component at some slices in Figure 6.4 at  $t=12\tau$ ,  $t=24\tau$ ,  $t=36\tau$ , and  $t=48\tau$ . The results of the IFE and FE methods are almost identical, demonstrating the effectiveness of the proposed method. In addition, we can clearly observe the delayed electromagnetic wave inside the torus agreeing with the physics. Next, we plot the electromagnetic fields inside the torus in Figure 6.5 such that we can also examine the direction. The plots still clearly show that the two methods have very similar simulation results.

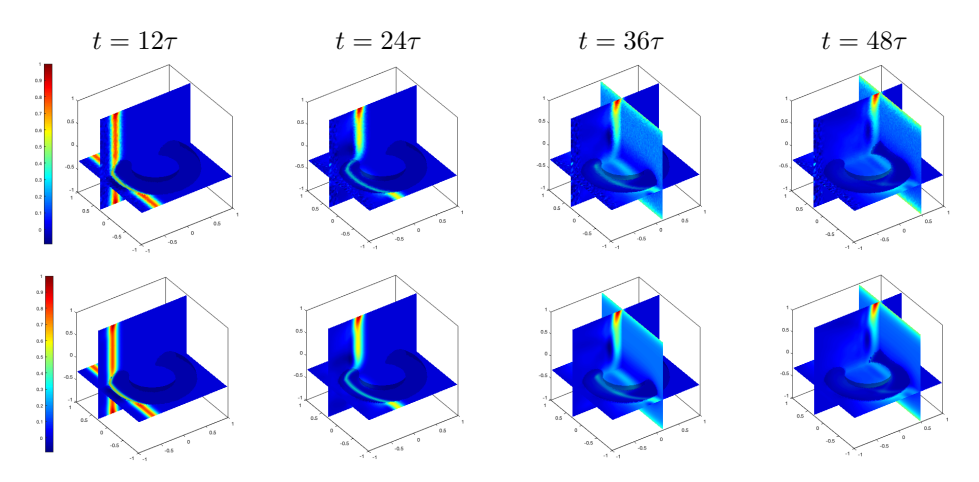


Fig. 6.4. Comparison of FE (top) and IFE (bottom) solutions at slices  $x_1 = 5/32$ ,  $x_2 = 5/16$ ,  $x_3 = -5/16$ .

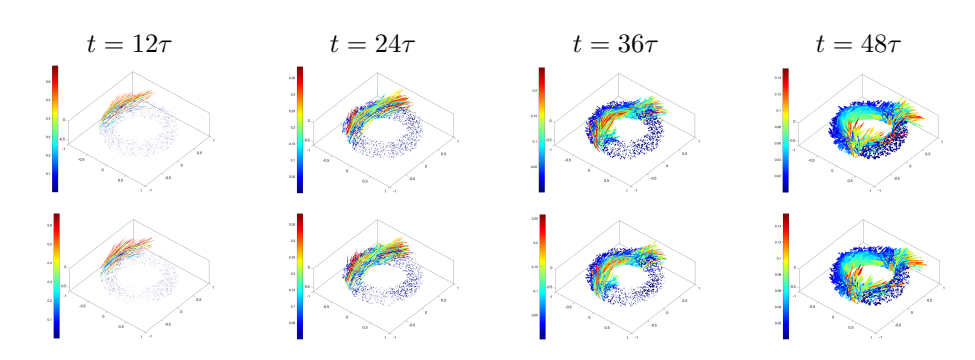


Fig. 6.5. Comparison of FE (top) and IFE (bottom) solutions of vector fields.

7. Concluding remarks. In this work, we have proposed an IFE method in a Petrov–Galerkin scheme for solving a  $\mathbf{H}(\text{curl})$  interface system. This type of interface problem is much more challenging than the usual  $H^1$  interface problems due to the low regularity. The proposed method can overcome the issue of suboptimal convergence caused by the nonconforming approximation spaces and the widely used penalty techniques. Nevertheless, it is also worthwhile to mention that, for the  $H^1$  elliptic interface problems, some suitable penalties may help in achieving numerical solutions robust to the high contrast of the discontinuous coefficients; see the discussion in [16, 29, 44, 55]. However, to the best of our knowledge, we are not aware of any work that deals with high-contrast Maxwell-type interface problems. It is indeed interesting and critical to study those problems as they widely appear in practice. Note that in some situations  $\beta$  may vanish on one medium but may not vanish on another medium.

Another contribution of this work is to develop an efficient preconditioner for the considered lowest-order case. We point out that it can be more challenging to develop preconditioners for high-order FE methods. Existing works can be found for solving Maxwell equations with standard FE methods, say [70, 72, 11, 4]. However, there seems no result in the literature for unfitted mesh methods.

Developing such an efficient solver is of great importance, especially for the high-frequency case [10].

Reproducibility of computational results. This paper has been awarded the "SIAM Reproducibility Badge: code and data available", as a recognition that the authors have followed reproducibility principles valued by SISC and the scientific computing community. Code and data that allow readers to reproduce the results in this paper are available in https://github.com/lyc102/ifem OR in the Supplementary Materials.

**Acknowledgment.** We would like to thank the anonymous reviewers for their constructive comments and suggestions on improving this article.

## REFERENCES

- [1] H. AMMARI, J. CHEN, Z. CHEN, D. VOLKOV, AND H. WANG, Detection and classification from electromagnetic induction data, J. Comput. Phys., 301 (2015), pp. 201–217.
- [2] D. N. ARNOLD, R. S. FALK, AND R. WINTHER, Preconditioning in H(div) and applications, Math. Comp., 66 (1997), pp. 957–984.
- [3] I. Babuška, G. Caloz, and J. E. Osborn, Special finite element methods for a class of second order elliptic problems with rough coefficients, SIAM J. Numer. Anal., 31 (1994), pp. 945– 981, https://doi.org/10.1137/0731051.
- [4] A. T. BARKER AND T. KOLEV, Matrix-free preconditioning for high-order H(curl) discretizations, Numer. Linear. Algebra Appl., 28 (2021), e2348.
- [5] K.-J. Bathe, The inf-sup condition and its evaluation for mixed finite element methods, Comput. & Structures, 79 (2001), pp. 243-252.
- [6] R. BECKER, E. BURMAN, AND P. HANSBO, A Nitsche extended finite element method for incompressible elasticity with discontinuous modulus of elasticity, Comput. Methods Appl. Mech. Engrg., 198 (2009), pp. 3352–3360.
- [7] L. BEIRÃO DA VEIGA, F. DASSI, G. MANZINI, AND L. MASCOTTO, Virtual elements for Maxwell's equations, Comput. Math. Appl., 116 (2022), pp. 82–99.
- [8] L. Beirão da Veiga and L. Mascotto, Interpolation and stability properties of low-order face and edge virtual element spaces, IMA J. Numer. Anal., 43 (2023), pp. 828–851.
- F. Ben Belgacem, A. Buffa, and Y. Maday, The mortar finite element method for 3D Maxwell equations: First results, SIAM J. Numer. Anal., 39 (2001), pp. 880–901, https://doi.org/10.1137/S0036142999357968.
- [10] M. BONAZZOLI, V. DOLEAN, I. G. GRAHAM, E. A. SPENCE, AND P.-H. TOURNIER, Domain decomposition preconditioning for the high-frequency time-harmonic Maxwell equations with absorption, Math. Comp., 88 (2019), pp. 2559–2604.
- [11] M. BONAZZOLI, V. DOLEAN, R. PASQUETTI, AND F. RAPETTI, Schwarz preconditioning for high order edge element discretizations of the time-harmonic Maxwell's equations, in Domain Decomposition Methods in Science and Engineering XXIII, C.-O. Lee, X.-C. Cai, D. E. Keyes, H. H. Kim, A. Klawonn, E.-J. Park, and O. B. Widlund, eds., Springer International Publishing, Cham, 2017, pp. 117–124.
- [12] J. R. Brauer, J. J. Ruehl, M. A. Juds, M. J. V. Heiden, and A. A. Arkadan, Dynamic stress in magnetic actuator computed by coupled structural and electromagnetic finite elements, IEEE Trans. Magn., 32 (1996), pp. 1046-1049.
- [13] S. C. Brenner, J. Cui, F. Li, and L.-Y. Sung, A nonconforming finite element method for a two-dimensional curl-curl and grad-div problem, Numer. Math., 109 (2008), pp. 509-533.
- [14] A. BUFFA, M. COSTABEL, AND M. DAUGE, Algebraic convergence for anisotropic edge elements in polyhedral domains, Numer. Math., 101 (2005), pp. 29-65.
- [15] E. Burman, S. Claus, P. Hansbo, M. G. Larson, and A. Massing, CutFEM: Discretizing geometry and partial differential equations, Internat. J. Numer. Methods Engrg., 104 (2015), pp. 472–501.
- [16] E. Burman, J. Guzmán, M. A. Sánchez, and M. Sarkis, Robust flux error estimation of an unfitted Nitsche method for high-contrast interface problems, IMA J. Numer. Anal., 38 (2018), pp. 646–668.
- [17] Z. CAI AND S. CAO, A recovery-based a posteriori error estimator for H(curl) interface problems, Comput. Methods Appl. Mech. Engrg., 296 (2015), pp. 169–195.

- [18] Z. CAI, R. LAZAROV, T. A. MANTEUFFEL, AND S. F. McCormick, First-order system least squares for second-order partial differential equations: Part I, SIAM J. Numer. Anal., 31 (1994), pp. 1785–1799, https://doi.org/10.1137/0731091.
- [19] S. CAO, L. CHEN, AND R. GUO, A virtual finite element method for two dimensional Maxwell interface problems with a background unfitted mesh, Math. Models Methods Appl. Sci., 31 (2021), pp. 2907–2936.
- [20] S. CAO, L. CHEN, AND R. GUO, Immersed virtual element methods for electromagnetic interface problems in three dimensions, Math. Models Methods Appl. Sci., 33 (2023), pp. 455–503.
- [21] R. CASAGRANDE, R. HIPTMAIR, AND J. OSTROWSKI, An a priori error estimate for interior penalty discretizations of the curl-curl operator on non-conforming meshes, J. Math. Ind., 6 (2016), 4.
- [22] R. CASAGRANDE, C. WINKELMANN, R. HIPTMAIR, AND J. OSTROWSKI, DG treatment of non-conforming interfaces in 3D Curl-Curl problems, in Scientific Computing in Electrical Engineering, Springer International Publishing, Cham, 2016, pp. 53-61.
- [23] D. CHAPELLE AND K. BATHE, The inf-sup test, Comput. & Structures, 47 (1993), pp. 537–545.
- [24] J. CHEN, Y. LIANG, AND J. ZOU, Mathematical and numerical study of a three-dimensional inverse eddy current problem, SIAM J. Appl. Math., 80 (2020), pp. 1467–1492, https://doi.org/10.1137/19M1282866.
- [25] L. CHEN, iFEM: An Integrated Finite Element Methods Package in MATLAB, Technical report, University of California at Irvine, 2009.
- [26] L. CHEN, H. WEI, AND M. WEN, An interface-fitted mesh generator and virtual element methods for elliptic interface problems, J. Comput. Phys., 334 (2017), pp. 327–348.
- [27] Z. CHEN, Q. Du, And J. Zou, Finite element methods with matching and nonmatching meshes for Maxwell equations with discontinuous coefficients, SIAM J. Numer. Anal., 37 (2000), pp. 1542–1570, https://doi.org/10.1137/S0036142998349977.
- [28] Z. CHEN, Y. XIAO, AND L. ZHANG, The adaptive immersed interface finite element method for elliptic and Maxwell interface problems, J. Comput. Phys., 228 (2009), pp. 5000–5019.
- [29] C.-C. CHU, I. G. GRAHAM, AND T.-Y. HOU, A new multiscale finite element method for highcontrast elliptic interface problems, Math. Comp., 79 (2010), pp. 1915–1955.
- [30] P. CIARLET, JR., AND J. ZOU, Fully discrete finite element approaches for time-dependent Maxwell's equations, Numer. Math., 82 (1999), pp. 193–219.
- [31] M. COSTABEL AND M. DAUGE, Singularities of electromagnetic fields in polyhedral domains, Arch. Ration. Mech. Anal., 151 (2000), pp. 221–276.
- [32] M. COSTABEL, M. DAUGE, AND S. NICAISE, Singularities of Maxwell interface problems, M2AN Math. Model. Numer. Anal., 33 (1999), pp. 627–649.
- [33] M. COSTABEL, M. DAUGE, AND S. NICAISE, Corner singularities of Maxwell interface and eddy current problems, in Operator Theoretical Methods and Applications to Mathematical Physics, Birkhäuser Basel, Basel, 2004, pp. 241–256.
- [34] F. DE PRENTER, C. V. VERHOOSEL, E. H. VAN BRUMMELEN, J. A. EVANS, C. MESSE, J. BENZAKEN, AND K. MAUTE, Multigrid solvers for immersed finite element methods and immersed isogeometric analysis, Comput. Mech., 65 (2020), pp. 807–838.
- [35] E. M. Dede, J. Lee, and T. Nomura, Multiphysics Simulation: Electromechanical System Applications and Optimization, Springer, 2014.
- [36] H. EDELSBRUNNER, Triangulations and meshes in computational geometry, Acta Numer., 9 (2000), pp. 133–213.
- [37] S. GROSS AND A. REUSKEN, An extended pressure finite element space for two-phase incompressible flows with surface tension, J. Comput. Phys., 224 (2007), pp. 40–58.
- [38] S. GROSS AND A. REUSKEN, Analysis of optimal preconditioners for CutFEM, Numer. Linear. Algebra Appl., (2022), e2486.
- [39] R. Guo, Solving parabolic moving interface problems with dynamical immersed spaces on unfitted meshes: Fully discrete analysis, SIAM J. Numer. Anal., 59 (2021), pp. 797–828, https://doi.org/10.1137/20M133508X.
- [40] R. Guo and T. Lin, An immersed finite element method for elliptic interface problems in three dimensions, J. Comput. Phys., 414 (2020), 109478.
- [41] R. Guo, Y. Lin, and J. Zou, Solving two-dimensional H(curl)-elliptic interface systems with optimal convergence on unfitted meshes, European J. Appl. Math., 34 (2023), pp. 774–805.
- [42] R. Guo, Y. L. T. Lin, and Q. Zhuang, Error analysis of symmetric linear/bilinear partially penalized immersed finite element methods for Helmholtz interface problems, J. Comput. Appl. Math., 390 (2021), 113378.
- [43] R. Guo and X. Zhang, Solving three-dimensional interface problems with immersed finite elements: A-priori error analysis, J. Comput. Phys., 441 (2021), 110445.

- [44] J. GUZMÁN, M. A. SÁNCHEZ, AND M. SARKIS, A finite element method for high-contrast interface problems with error estimates independent of contrast, J. Sci. Comput., 73 (2017), pp. 330–365.
- [45] P. Hansbo, M. G. Larson, and S. Zahedi, A cut finite element method for a Stokes interface problem, Appl. Numer. Math., 85 (2014), pp. 90–114.
- [46] R. HIPTMAIR, J. LI, AND J. ZOU, Convergence analysis of finite element methods for H(div; Ω)elliptic interface problems, J. Numer. Math., 18 (2010), pp. 187–218.
- [47] R. HIPTMAIR, J. LI, AND J. ZOU, Convergence analysis of finite element methods for H(curl; Ω)-elliptic interface problems, Numer. Math., 122 (2012), pp. 557–578.
- [48] R. HIPTMAIR AND J. Xu, Nodal auxiliary space preconditioning in H(curl) and H(div) spaces, SIAM J. Numer. Anal., 45 (2007), pp. 2483–2509, https://doi.org/10.1137/060660588.
- [49] S. HOU, P. SONG, L. WANG, AND H. ZHAO, A weak formulation for solving elliptic interface problems without body fitted grid, J. Comput. Phys., 249 (2013), pp. 80–95.
- [50] T. Y. Hou, X.-H. Wu, and Y. Zhang, Removing the cell resonance error in the multiscale finite element method via a Petrov-Galerkin formulation, Commun. Math. Sci., 2 (2004), pp. 185–205.
- [51] P. HOUSTON, I. PERUGIA, A. SCHNEEBELI, AND D. SCHÖTZAU, Interior penalty method for the indefinite time-harmonic Maxwell equations, Numer. Math., 100 (2005), pp. 485–518.
- [52] P. HOUSTON, I. PERUGIA, AND D. SCHÖTZAU, Mixed discontinuous Galerkin approximation of the Maxwell operator, SIAM J. Numer. Anal., 42 (2004), pp. 434–459, https://doi.org/10.1137/S003614290241790X.
- [53] J. Hu And H. Wang, An optimal multigrid algorithm for the combining P<sub>1</sub>-Q<sub>1</sub> finite element approximations of interface problems based on local anisotropic fitting meshes, J. Sci. Comput., 88 (2021), 16.
- [54] Q. Hu, S. Shu, and J. Zou, A mortar edge element method with nearly optimal convergence for three-dimensional Maxwell's equations, Math. Comp., 77 (2008), pp. 1333-1353.
- [55] P. HUANG, H. WU, AND Y. XIAO, An unfitted interface penalty finite element method for elliptic interface problems, Comput. Methods Appl. Mech. Engrg., 323 (2017), pp. 439–460.
- [56] H. Ji, An immersed Crouzeix-Raviart finite element method in 2D and 3D based on discrete level set functions, Numer. Math., 153 (2023), pp. 279–325.
- [57] R. KAFAFY, T. LIN, Y. LIN, AND J. WANG, Three-dimensional immersed finite element methods for electric field simulation in composite materials, Internat. J. Numer. Methods Engrg., 64 (2005), pp. 940–972.
- [58] J. LI, J. M. MELENK, B. WOHLMUTH, AND J. ZOU, Optimal a priori estimates for higher order finite elements for elliptic interface problems, Appl. Numer. Math., 60 (2010), pp. 19–37.
- [59] R. Li, Q.-C. Liu, and F.-Y. Yang, A reconstructed discontinuous approximation on unfitted meshes to H(curl) and H(div) interface problems, Comput. Methods Appl. Mech. Engrg., 403 (2023), 115723.
- [60] T. Lin, Y. Lin, and X. Zhang, Partially penalized immersed finite element methods for elliptic interface problems, SIAM J. Numer. Anal., 53 (2015), pp. 1121–1144, https://doi.org/ 10.1137/130912700.
- [61] H. LIU, L. ZHANG, X. ZHANG, AND W. ZHENG, Interface-penalty finite element methods for interface problems in H<sup>1</sup>, H(curl), and H(div), Comput. Methods Appl. Mech. Engrg., 367 (2020), 113137.
- [62] T. LUDESCHER, S. GROSS, AND A. REUSKEN, A multigrid method for unfitted finite element discretizations of elliptic interface problems, SIAM J. Sci. Comput., 42 (2020), pp. A318– A342, https://doi.org/10.1137/18M1203353.
- [63] G. MAKINSON AND A. SHAH, An iterative solution method for solving sparse nonsymmetric linear systems, J. Comput. Appl. Math., 15 (1986), pp. 339–352.
- [64] P. Monk, Finite Element Methods for Maxwell's Equations, Oxford University Press, 2003.
- [65] J. C. Nedelec, Mixed finite elements in  $\mathbb{R}^3$ , Numer. Math., 35 (1980), pp. 315–341.
- [66] J. C. NÉDÉLEC, A new family of mixed finite elements in R<sup>3</sup>, Numer. Math., 50 (1986), pp. 57−81.
- [67] S. OSHER AND R. P. FEDKIW, Level set methods: An overview and some recent results, J. Comput. Phys., 169 (2001), pp. 463–502.
- [68] P. A. RAVIART AND J. M. THOMAS, A mixed finite element method for 2nd order elliptic problems, in Mathematical Aspects of Finite Element Methods, I. Galligani and E. Magenes, eds., Springer-Verlag, Berlin, New York, 1977, pp. 292–315.
- [69] K. ROPPERT, S. SCHODER, F. TOTH, AND M. KALTENBACHER, Non-conforming Nitsche interfaces for edge elements in curl-curl-type problems, IEEE Trans. Magn., 56 (2020), 7400707.
- [70] J. SCHOBERL AND S. ZAGLMAYR, High order Nédélec elements with local complete sequence properties, COMPEL, 24 (2005), pp. 374–384.

- [71] J. A. SETHIAN, Level Set Methods and Fast Marching Methods, 2nd ed., Cambridge Monogr. Appl. Comput. Math. 3, Cambridge University Press, Cambridge, 1999.
- [72] J. Wang, S. Shu, and L. Zhong, Efficient parallel preconditioners for high-order finite element discretizations of H(grad) and H(curl) problems, in Domain Decomposition Methods in Science and Engineering XIX, Y. Huang, R. Kornhuber, O. Widlund, and J. Xu, eds., Springer, Heidelberg, 2011, pp. 325–332.
- [73] S. WANG, F. WANG, AND X. Xu, A robust multigrid method for one dimensional immersed finite element method, Numer. Methods Partial Differential Equations, 37 (2021), pp. 2244– 2260.
- [74] T. WARBURTON AND J. S. HESTHAVEN, On the constants in hp-finite element trace inverse inequalities, Comput. Methods Appl. Mech. Engrg., 192 (2003), pp. 2765–2773.
- [75] J. Xu And Y. Zhu, Uniform convergent multigrid methods for elliptic problems with strongly discontinuous coefficients, Math. Models Methods Appl. Sci., 18 (2008), pp. 77–105.
- [76] J. Xu and J. Zou, Some nonoverlapping domain decomposition methods, SIAM Rev., 40 (1998), pp. 857–914, https://doi.org/10.1137/S0036144596306800.
- [77] S. ZHAO AND G. W. Wei, High-order FDTD methods via derivative matching for Maxwell's equations with material interfaces, J. Comput. Phys., 200 (2004), pp. 60–103.